

Contents

1 Neutron Measurements at IP2I cryogenic facility	1
1.1 Motivation	1
1.2 Experimental Setup	1
1.3 Pre-processing and Data format	3
1.4 Livetime Cut	5
1.5 Quality Cuts	8
1.6 Cross-talk Correction	10
1.7 Calibration	12
1.8 Charge conservation cut	15
1.9 Fiducial Cut	17
1.10 Band cut	21
1.11 Pulse simulation	24
1.12 Trigger cut	26
1.13 Band Contamination Correction	28
1.14 Efficiency correction	30
1.15 Normalization of the energy spectra	32
1.16 Measurement of the ILL neutron background	33
1.17 Study of the Heat-Only events	34
1.18 Rejection and Leakage	35

Chapter 1

Neutron Measurements at IP2I cryogenic facility

PERSONNAL REF [see Neutron measurements at IP2I with Ge bolometers.pdf]

<https://elog.ipnl.in2p3.fr/manoir/R%26D+Cryo+LIO/51>

WEAK REF

[see NeutronMeasurementCampaign.pdf]

OFNote.pdf

STRONG REF

68Ge-68Ga-Decay.pdf

1.1 Motivation

As the Ricochet experiment is happening near a nuclear reactor, there is a risk that the bolometers will be blinded by the radioactive background of the site. The radioactive background is mainly composed of particles inducing electronic recoil (such as gammas, electrons, muons, charged particles essentially) and neutron producing nuclear recoils. While the former background component can be discriminated thanks to technology used in the bolometers, the latter can not and thus constitute an unavoidable background for Ricochet which will limit the CENNS process measurement. Therefore, it is vital to evaluate the neutron background on-site and understand its dependency in the energy. In addition to estimating the limitations on the measurement, the study of the neutron background on-site will also be used in the design of the shielding.

The actual measurement of the neutron background at the ILL site [1.1b](#) was achieved with gaseous Helium-3 Tube Detector based on the neutron capture by ^3He :



This detector technology is sensitive to thermal/fast? neutron at high energy >MeV which is order of magnitude superior to the energy range of the cryogenic germanium bolometers. The estimation of the neutron background at ILL in the energy range of interest is then obtained by extrapolation of the neutron background at IP2I validated with relative measurements between the tube detector and the germanium detector technology.

1.2 Experimental Setup

Two subsections: RED80 detector (describing RED80, sensitivity, electric field, polarization), Operation in cryostat (describing the temperature, the suspended tower, the configuration Calibration and Background, the calendar of the streams)

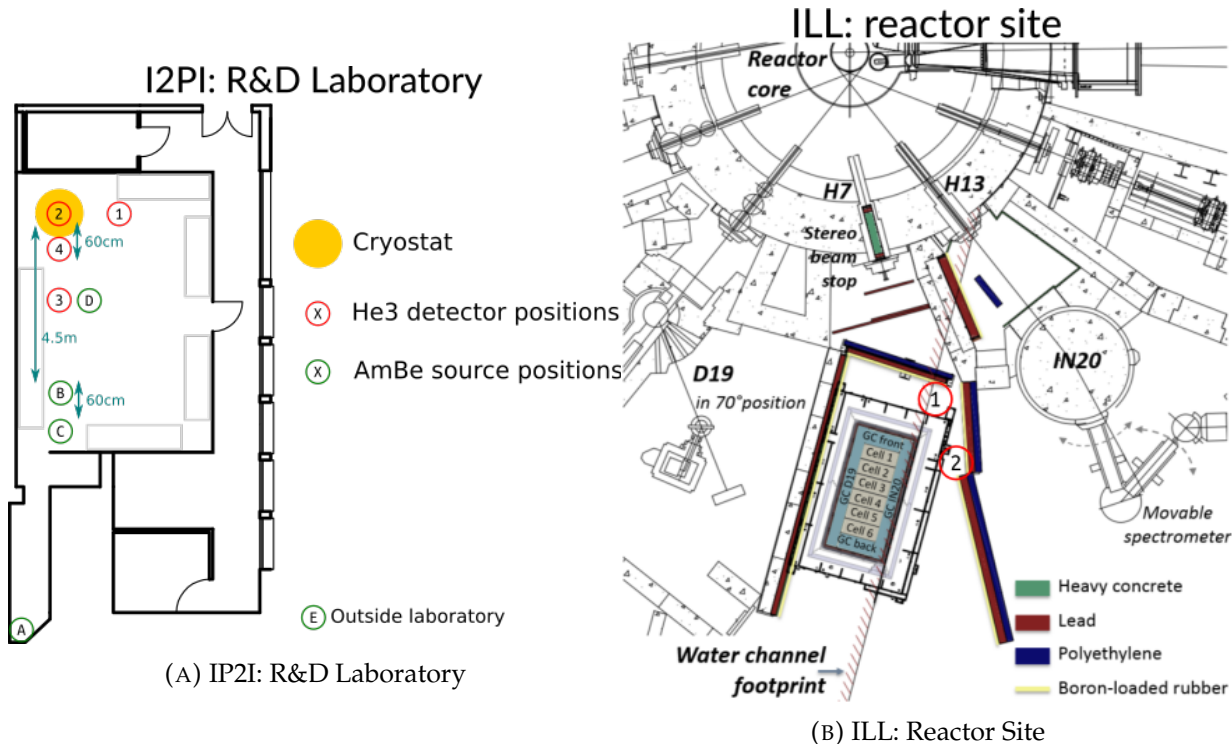


FIGURE 1.1: Schemes of the neutron background measurements site with ^3He gaseous detectors. The positions of the detectors and the neutron source are indicated with numbered/colored tokens.

The measurement of the neutron background at the IP2I cryogenic facility was done with a newly designed low-threshold germanium detector of the RED series called RED80 with RMS resolution of approximately 120eV on the heat channel and 200eV on the ionization channel. The data were taken during the run 57 which began on 03/07/2019 and ended on 01/08/2019. In this run, RED80 and RED70 were both operated on the suspended tower.

RED80 is composed of a 38g cylindrical germanium crystal of height 10mm and diameter 30mm. It is equipped with a heat channel and an ionization channel (see figure 1.2) The ionization channel consists of a pair of collecting electrodes and guard electrodes. The collecting electrodes are two flat full aluminium electrodes of diameter 27mm deposited on its top and bottom surface. The guard electrodes are four circular electrodes deposited on its side. The heat channel consists of a NTDGe thermistance labeled K58 with dimension 4*4*0.45 mm. Before being installed into the cryostat, the detector was placed near a neutron source in order to activate the Germanium crystal and benefit from the intrinsic gamma calibration peak during operation. The neutron activation started on 28/06/2019 at 17h08 and ended on 02/08/2019 at 10h08 yielding 89h of activation.

From 08/08/2019, the detectors were characterized at 18mK. As for the actual condition of the neutron background measurements, RED80 was operated at 16mK with an optimal NTD polarization current of 1nA and an electric potential difference of 2V on the ionization channel:

$$A, B, C, D = +1, +1, -1, -1.$$

The data taking was divided between two configurations, "Background" and "Calibration", meant to measure the neutron background and calibrate the neutron recoil band in the detector respectively. The Background configuration was used to save 34 hours of data partitioned in three streams: tg18l005, tg27l000 and tg28l000. The Calibration configuration was used to take 78 hours of data, with an Americium-Beryllium neutron source situated 4.5m away from the

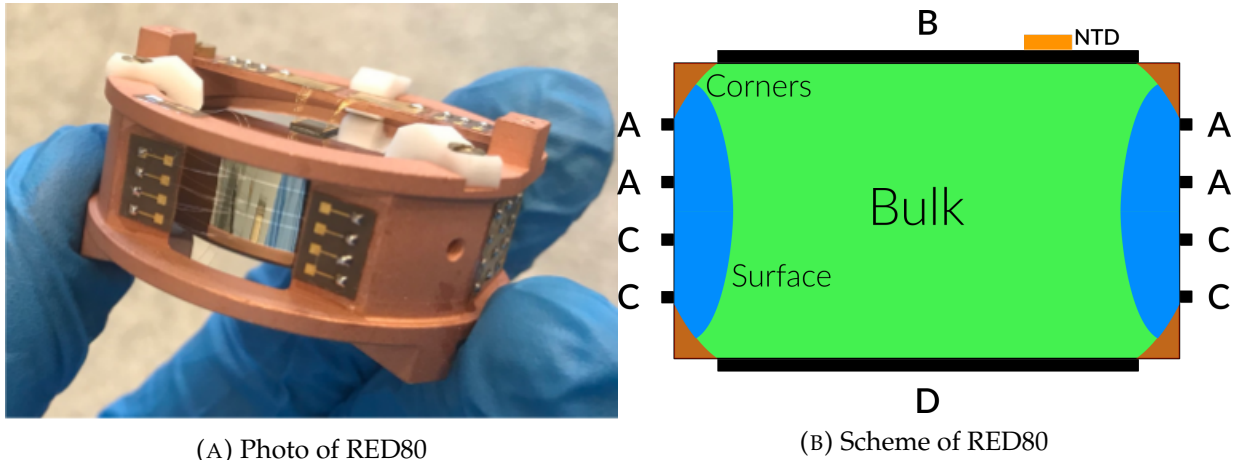


FIGURE 1.2: Description of RED80, with a schematic drawing of the Germanium crystal, the NTD sensor and the position and polarization of the electrodes.

Configuration	Stream	Started at
Background	tg18l005	?? on 18/08/2019
	tg27l000	21h20 on 27/08/2019
	tg28l000	11h27 on 28/08/2019
Calibration	tg17l007	?? on 17/08/2019
	tg19l010	17h10 on 19/08/2019
	tg20l000	?? on 20/08/2019
	tg21l000	?? on 21/08/2019

TABLE 1.1: Starting hours and date of the streams for neutron background and calibration measurements.

cryostat and shielded with milk (acting as water) to thermalize the emitted neutron (see figure ??). The data were saved in four streams: tg17l007, tg19l010, tg20l000 and tg21l000.

Each stream was taken during nights or week-ends to benefit from the long time with stable operation (see Table 1.1). The configurations were mixed in term of dates, which is of importance when measuring the rate of the Germanium calibration peaks which is decreasing with time.

1.3 Pre-processing and Data format

The data were initially saved as streams: the voltage value of the heat channel and the four ionization channel are saved for each time step in the acquisition with a sampling frequency of 400Hz.

FIGURE STREAM HEAT/IONIZATION

These voltage values are extracted by an analog-to-digital conversion system and thus expressed in Analog-to-Digital conversion Unit (ADU). These data streams are then processed by an Optimal Filtering (OF) software called NEPAL. A filter based on the signal PSD and the noise PSD in the bolometer is applied to the stream. Time windows of 1s centered on a triggering events are selected with an amplitude threshold on the filtered stream (see Figure 1.4).

These time windows are processed to extract several quantities:

- Timestamp,
- Amplitude (filtered decorrelated),

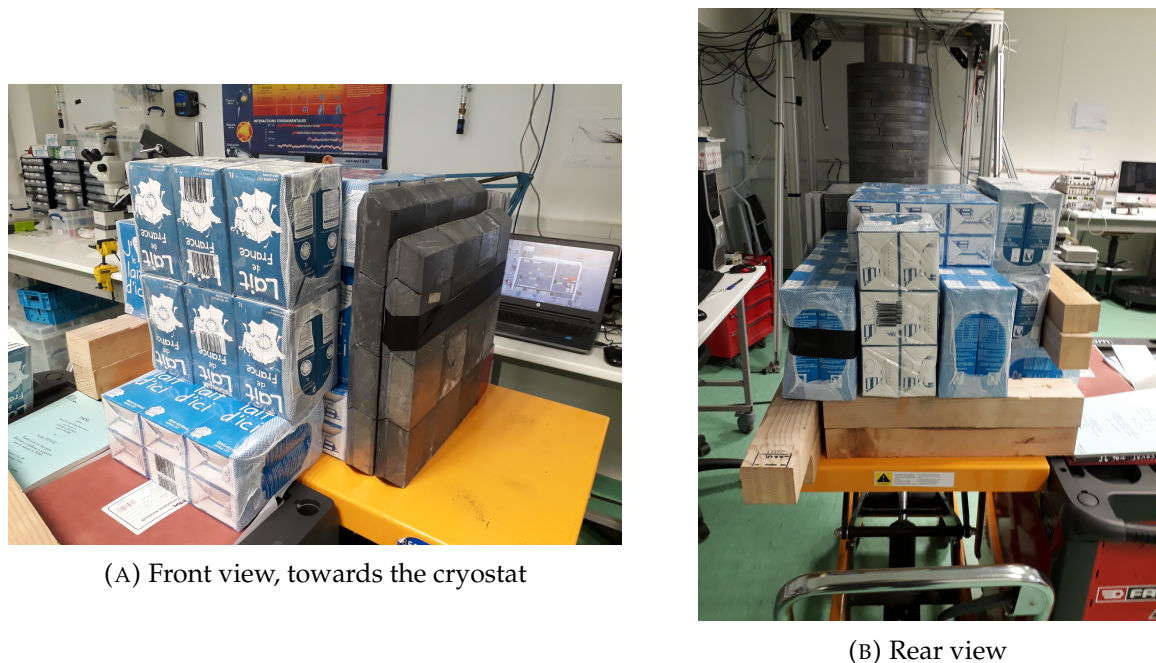


FIGURE 1.3: Photo of the shielded AmBe neutron source used for the neutron calibration.

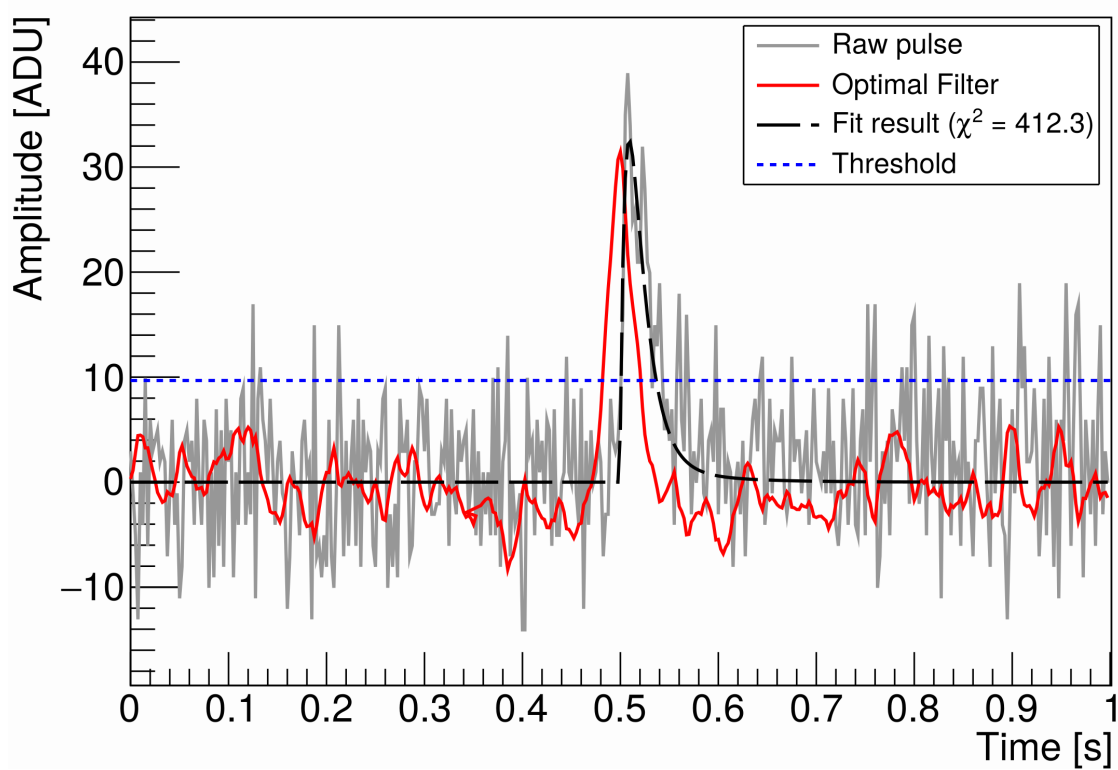


FIGURE 1.4: Optimal filtering of a 1s pulse window.

- Chi2 value (filtered decorrelated),
- Offset (raw),
- Ionization Slope (raw),

The figure 1.6 shows this characterization quantities for each triggering event as a function of their timestamp (for the considered stream, here tg17l007). Each scatter plots is understood when applying the quality cut:

- Heat Energy vs Timestamp: Reconstruction of the energy deposited in the heat channel for each event. This graph can be linked to the heat energy spectrum presented later. One can note pronounced population of fixed energy corresponding to the abundance of 10.37keV events due to the activation of the Germanium crystal and the noise blob poulation at $\mathcal{O}(50)$ eV.
- Ionization Energy vs Timestamp: is quite the same as heat energy, except that with the overlap of the different channels this graph is now an useless mess
- Offset Heat vs Timestamp: this curve is proportional to the resistance value of the NTD sensor and allows us to follow the baseline temperature. With this decreasing profile, we deduce that the detector has been cooling during this stream. Note that although RED80 is still slowly thermalizing, the sensitivity is stable (precision?)
- Offset Ionization vs Timestamp: this curve is essentially used to discard all the events with an offset outside of the $[-14000, 14000]$ ADU (see 1.5).
- Slope Ionization vs Timestamp: this curve is proportional to the baseline current measured by each electrodes. This baseline current is explained by the presence of leakage current between the electrodes (dedicated section?) and the collection of trapped charges (especially after a maintenance).
- Chi2 vs Timestamp: This describes the goodness of the fit of the template to the pulse. A stable low value indicate a fixed shape for the pulses, which is required for the chi2 cut applied later (see 1.5)

In the end, for each configuration of data measurements(Background and Calibration), triggering events were selected in each streams and described by several quantities. Among those triggering events are events of interest well reconstructed and induced by electronic recoil from the radioactive gamma background, the KLM activation lines from the germanium and the cosmic muons and neutron recoil from the AmBe neutron source and the radioactive neutron background. However, many triggering events can not be reconstructed or were induced by parasitic source, and can not yield information for the measurement of the neutron background at IP2I. To extract the events of interest from all the data, analysis cuts are applied.

1.4 Livetime Cut

The livetime corresponds to the period of time where the detector is considered available for data taking. It is important to consider the appropriate livetime for a stream as all the results presented in the analysis will eventually be weighted by the exposure of the detector and so this very livetime. While we would like the livetime to corresponds to the running time of the detector, it is often not the case. There can be some periods where the temperature regulation of the cryostat can be defective (temperature spikes, power cuts) which degrade the heat sensitivity of the detector, and other periods where various malfunctions can prevent the saving of data all

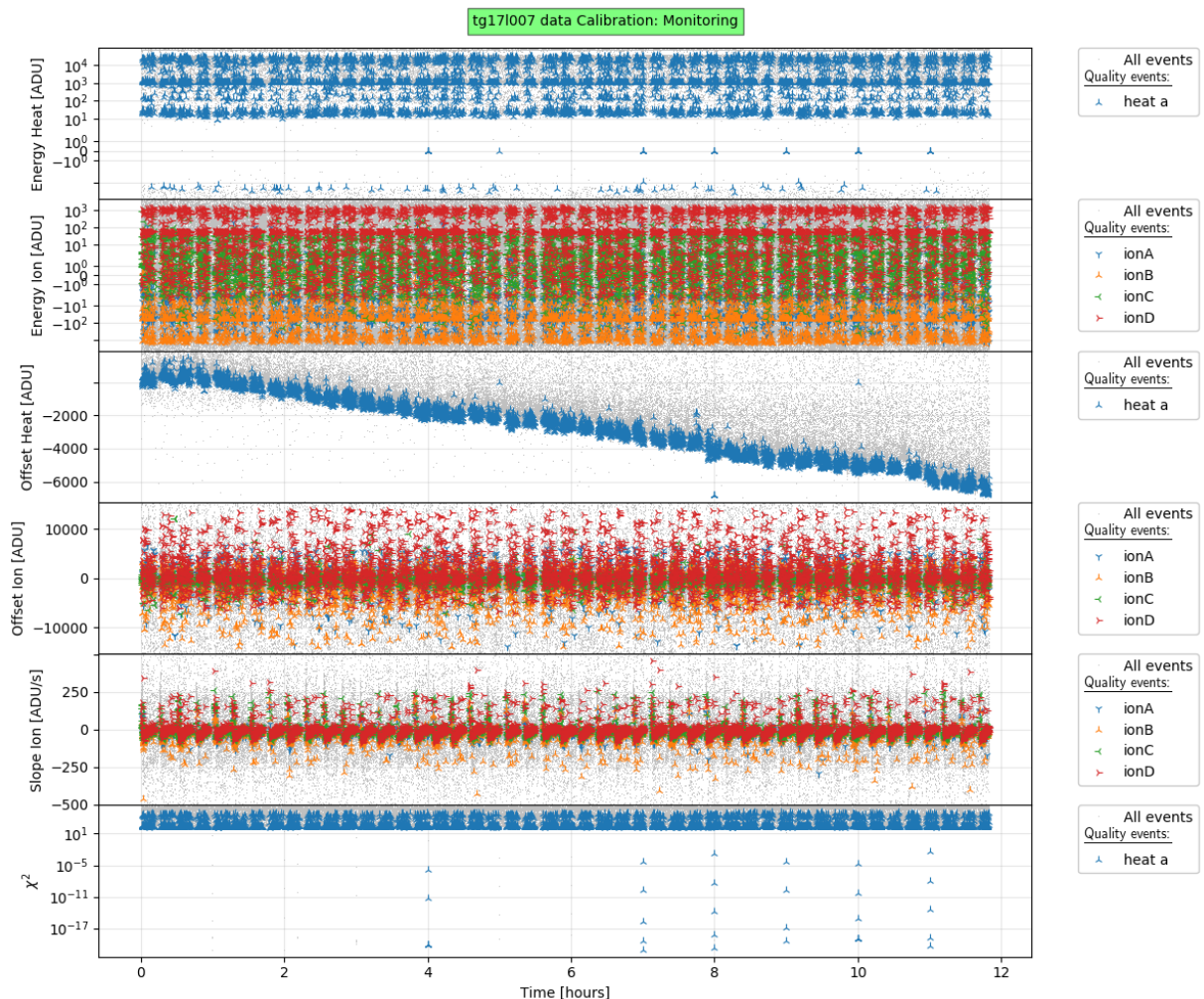


FIGURE 1.5: Characterization quantities of triggering events as a function of their timestamp. (TO BE CHANGE !)

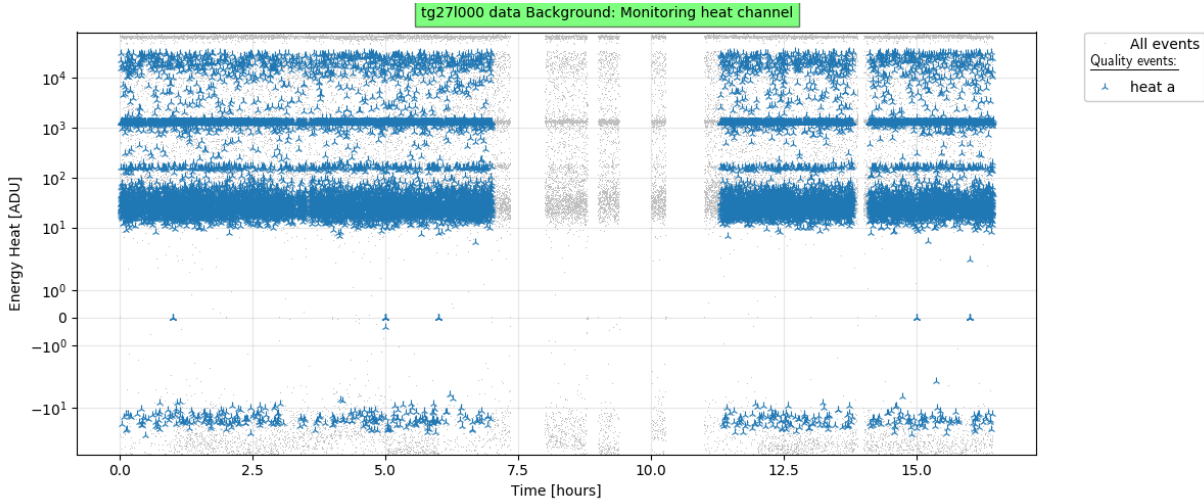


FIGURE 1.6: Reconstructed amplitude on the heat channel in function of the timestamp for every events of the stream "tg27l000". All events are plotted in grey while events passing the "Livetime" are in blue.

Stream	Time Interval [hours]		Time length [hours]		Livetime Percentage	Configuration	Livetime
	Raw	Fine	Raw	Fine			
tg17l007	[0, 11.83]	[0, 11.83]	11.83	11.83	100%	Calibration	75.6
tg19l010	[0, 20.86]	[0, 8.3] \cup [8.7, 20.86]	20.86	20.47	98.1%		
tg20l000	[0, 26.37]	[0, 26.37]	26.37	26.37	100%		
tg21l000	[0, 16.93]	[0, 16.93]	16.93	16.93	100%		
tg18l005	[0, 14.95]	[0, 7.4] \cup [7.6, 14.95]	14.95	14.75	98.7%	Background	35.93
tg27l000	[0, 16.43]	[0, 7] \cup [11.3, 13.8] \cup [14.1, 16.43]	16.43	11.83	72.0%		
tg28l000	[0, 21.50]	[0, 7.4] \cup [8.05, 10]	21.50	9.35	43.5%		

TABLE 1.2: Calculation of the livetime of every stream. Fine time intervals were estimated visually from monitoring plots (as in figure 1.6) with precautionary buffers. The "Livetime cut" keeps all the events with timestamps in the selected fine intervals. The total lifetime of both configuration is used in the calculation of the exposure of the RED80.

together. The stability of the detector operation is monitored for each streams with a graph of the energy amplitude of the events in function of their timestamp. Such a graph is plotted in the figure 1.6 for the stream "tg27l000".

It appears that RED80 was operated at a constant temperature for the duration of this stream (this is also observed for all the other streams). Indeed, the events corresponding to the calibration peaks are reconstructed with a fixed amplitude (approximately 2×10^2 ADU for the 1.3keV and 2×10^3 ADU for the 10.37keV), and thus we check that the sensitivity of the heat channel is constant for the whole stream.

However, some strange periods of time are visible where no events were saved. In the presented figure, it is most notable in the intervals [7,11.3] and [13.8,14.1] hours. These portions of the streams were corrupted or rendered useless for reasons not clearly understood relative to the acquisition electronics.

The livetime is visually deduced from this monitoring plot for each stream and presented in the table 1.2.

The raw streams have various "fine" time intervals where the data can be taken properly. These fine intervals define the so-called "Livetime cut" which discarded any events not in the fine intervals. In the figure 1.6, all the events are plotted in gray while only the events passing the Livetime cut are plotted in blue. The intervals were chosen with some precautionary buffer in to apply a conservative cut that would reject any abnormal event. In the end, the livetime is

obtained for each streams and added for both configuration, giving a livetime of 75.6 hours for the Calibration and 35.93 hours for the Background.

1.5 Quality Cuts

The objective of the "Quality cut" is to keep the events induced by recoils in the germanium absorber of RED80 and with a good energy reconstruction. These events passing the Quality cut are labeled as "quality events" and satisfy several criteria:

- passing the Livetime Cut,
- not happening during a maintenance period of the ionization channel,
- offset of the ionization channel in the $[-14000, +14000] \text{ADU}$ interval,
- the χ^2 value, expressing the goodness of the fit of the event with the signal template.

Maintenance cut paragraph, will surely be moved in the section describing the electronics.

The electrodes of the ionization channel are collecting the electron-hole pairs induced by the recoils in the germanium crystal. As a results, their electric potential is decreasing (recall $Q = CU$) as well as the electric field guiding the e-h pairs in the crystal. In order to keep a steady electric field, it is necessary to periodically recharge the electrodes, offsetting the effect of the e-h pairs collection. This process is called "Reset" and is usually set to happen every few seconds in detectors. An adverse effect of these resets is that they usually induce a signal on the heat and ionization channels. While these signals are easily discarded using their known frequency, they can happen close to a valid signal resulting in a pile-up, the discarding of the event from the analysis, and so a decrease in the livetime of a data stream.

Another phenomenon degrading the electric field is the trapping of the charges in the crystal. Even if the electrodes are properly "resetted", the accumulating trapped charges produces a counter-field effectively reducing the electric field seen by the e-h pairs in the crystal. The method used to even the charges in the crystal is called "Maintenance". The electrodes are successively polarized at plus and minus their nominal electric potential with a frequency of $\mathcal{O}(1\text{Hz})$ for about a minute. The trapped charges are shaken up in the crystal and eventually recombine or are collected at the electrodes. The counter-field vanishes and the detector is ready to operate with its standard electric field (graph necessary to illustrate ?). A downside is that the detector is not available for data taking during a maintenance, representing about a minute of deadtime for several tenths of minutes of running time.

As this work uses data taken with detectors operated in an above-ground laboratory, the event rate is higher compared to an underground facility due to the abundance of cosmic rays and the natural radioactivity. With this higher event rate comes a higher charge collected per unit of time. This induces a quicker decrease of the electric potential of the electrodes, which needs for more frequent resets, and a quicker appearing of the counter-field due to the charge trapping, which calls for more frequent maintenances.

Thus, the frequency of the reset and the maintenance is adapted to the event rate seen by the detectors. The reset and maintenance should be frequent enough to keep up with the electric field decrease, yet spaced out to keep a reasonable livetime. Moreover, the event rate do fluctuate between each run as it depends on the mass of the absorbers (here 32g, 38g or 200g) and the possible use of calibration sources increasing the event rate (see the section ??). In average in this work, the resets are set to a frequency of 2Hz (?) and maintenance set to take place every 40 minutes. **End of Maintenance paragraph**



FIGURE 1.7: Graph of the reconstructed amplitude of the ionization channels in function of their offset value. The data presented corresponds to the stream "???".
Should illustrate the sensitivity degradataion going past approx 1400 ADU.

Quality events should not happen during a maintenance period nor a reset (introduced in section 1.5 as they are considered electronics artifacts. The "Maintenance cut" is defined as:

blibloubloup

which discards any event happening during a maintenance period. The "Reset cut" is expressed as:

hellogeneral

which discards event occurring within 5ms (?) of a reset. **INSERT MATHEMATICAL DEFINITION of the maintenance cut and the reset cut. And implement it correctly in the analysis!**

paragraph about the ion sensitivity degradation past 14000ADU. Dont know if this is gonna stay in this chapter or move it when describing the electronics. Feel like it should belong here, as I can illustrate that with a figure

We noticed a malfunction for the ionization channel: apparently, the sensitivity of the ionization channels depends on their offset value. This behavior is consider as faulty as we expect the electrodes to have a constant sensitivity. This phenomenon is illustrated in the figure 1.7 which plots the ionization amplitudes of events as a function of their offset values for the data stream "???".

INTERPRETATION when plot is ready. We decide to keep the events with the standard ionization sensitivity with low absolute offset value. Other events are discarded by the "Offset cut" which is expressed as:

mathemeticshere

Concerning the χ^2 value, the threshold depends on the energy. Indeed, because of non-linearity in the bolometer heat response, the shape of the signal do depends on the recoil energy as the first order perturbation theory becomes less and less valid. Good events at low energy should have a χ^2 value of about:

$$\mathbb{E}(\chi^2) = N_{\text{samples in window}} = T_{\text{window}} \times f_{\text{sampling}} = 0.5 \times 400 = 200 \quad (1.2)$$

However, with a signal template based on events from the 10.37keV activation line of the germanium, the χ^2 value of good events is increasing from $\mathcal{O}(10\text{keV})$. Therefore, a cut parametrization function depending on the event amplitude is chosen:

Channel type	α	β	Streams	γ
Heat	2×10^3	2	tg17l007	1
			tg18l005	1
			tg19l010	1
			tg20l000	1
			tg21l000	1
			tg27l000	1.75
			tg28l000	1.75
Ionization	3×10^2	2.2	All	1

TABLE 1.3: Coefficient of the χ^2 cut for each streams. These coefficients were determined visually in order to defined the band of events of lowest χ^2 value on the whole energy range.

$$\text{Threshold}(Amplitude) = \gamma \times \mathbb{E}(\chi^2) \times \left[1 + \left(\frac{Amplitude}{\alpha} \right)^\beta \right] \quad (1.3)$$

with α , β and γ estimated visually for each streams and presented in table 1.3.

In the end, the χ^2 cut is applied on each channels (as seen in figure 1.8) independently. Only the events passing the cut for all the channels is kept and eligible as a quality event.

With all these criteria being applied to the events passing the Livetime Cut, we have selected the events passing the Quality Cut, qualified as "quality events".

1.6 Cross-talk Correction

While the heat channel can readily be calibrated, this is not the case for the ionization channel which are affected by a phenomenon of cross-talk which should be corrected before proceeding with their calibration. Because of the capacitive coupling between the different electrodes of the bolometer, a signal collected by an electrode will induce another smaller signal on other electrodes. With such a coupling, the cross-talk factor between two electrodes increases with their associated capacitance term. As a result, for a small bolometer as RED80 with capacitance terms in (O)($10pF$), the cross-talk factors are about few percents. This is to be compared to the bigger 200g FID bolometers used in EDELWEISS-III, with an increased capacitance of (O)($100pF$), presenting cross-talk factors of about few tens of percent. The real ionization channels A, B, C, D affected by the crosstalk can be corrected into decoupled ionization channels A', B', C', D' according to the following equation:

$$\begin{bmatrix} A' \\ B' \\ C' \\ D' \end{bmatrix} = \mathcal{M} \begin{bmatrix} A \\ B \\ C \\ D \end{bmatrix} \quad (1.4)$$

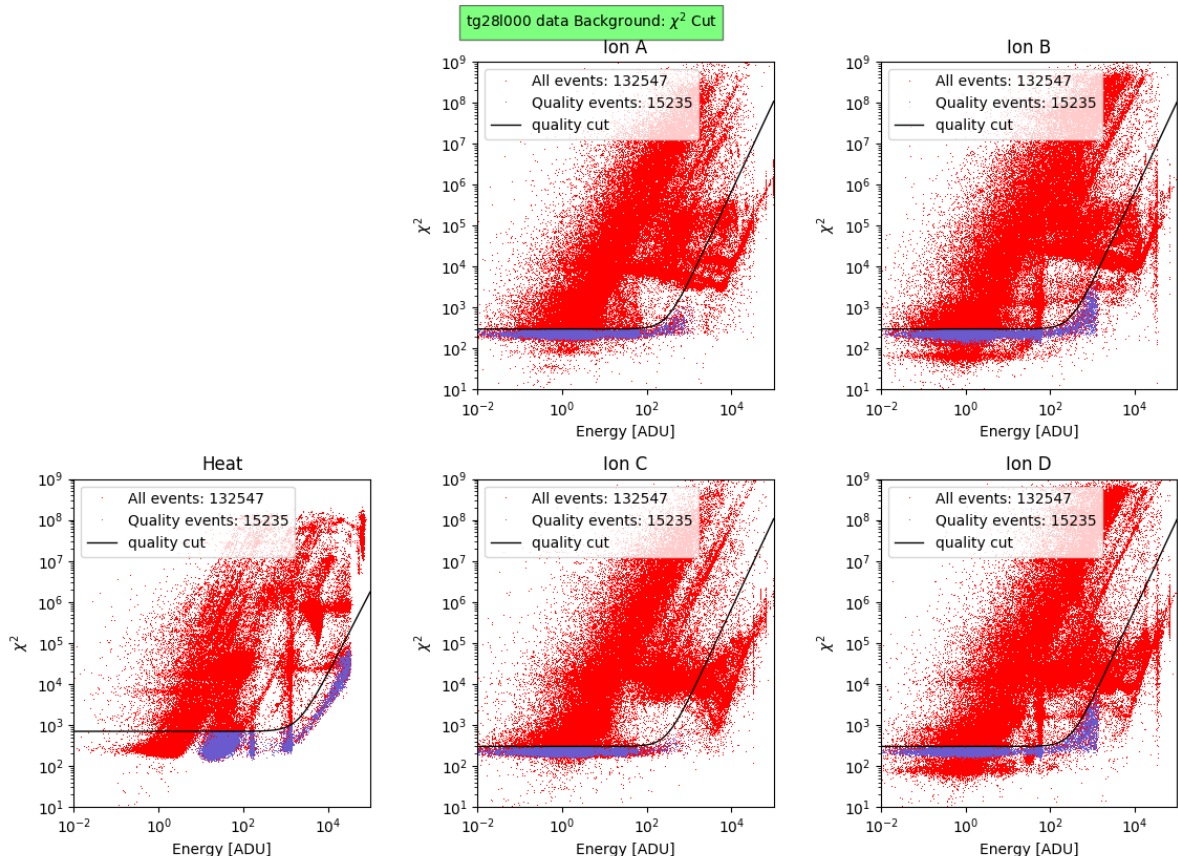


FIGURE 1.8: χ^2 value for each event in function of its reconstructed amplitude for the five measuring channels. The cut threshold is represented by the black line. All events are in red, passing events are in blue.

with \mathcal{M} the cross-talk correction matrix being:

$$\mathcal{M} = \begin{bmatrix} 1 & -0.052 & 0 & 0 \\ -0.03 & 1 & 0 & 0 \\ -0.012 & 0.001 & 1 & -0.025 \\ 0 & 0 & -0.03 & 1 \end{bmatrix} \quad (1.5)$$

The terms of this correction matrix were found with the study of specific populations of events of known characteristics (as seen in figure 1.2b):

- Bulk events are collected by the main electrodes and no charge is collected by the guard electrodes with

$$A' = C' = 0$$

- Surface events are collected by the guard electrodes and no charge is collected by the main electrodes with

$$B' = D' = 0$$

This correction is implemented iteratively by visually checking the plotting of the corrected ionization channels against themselves. The figure 1.9 shows the signals of the events of the uncorrected ionization channels A, B, C, D as black points. Superposing to this are the blue points associated with the events of the decoupled ionization channels A', B', C', D' .

We check that the cross-talk correction matrix \mathcal{M} corresponds to the identity matrix at the first order. The correction terms are in the range of few percents, going up to 5.2% in the case of the case of the electrode B inducing signal on the electrode A .

1.7 Calibration

The five measurements channels are saving the voltage of their associated sensors in ADU unit specific to each considered channel. In order to proceed with physical interpretation, it is now necessary to convert the channels into a common unit. For this purpose, we use the activation of the KLM lines of the Germanium crystal, which emits a gamma of energy 100eV, 1.3keV and 10.37keV respectively [[3]]. This gammas of known energy produce electronic recoils depositing a known energy in the ionization channels and the heat channel, with the latter being boosted with the Luke-Neganov effect [[2] and [1]]. As the quenching of the electronic recoil is different from the one of the nuclear recoil, we use the keV_{ee} which precise that the energy deposit done with an electronic recoil.

Concerning the ionization channels, we use the 10.37keV line forming a multivariate normal distributed blob in the figure 1.10 showing the signal of an event in each ionization channel in ADU unit. We estimate the center of this distribution to be 55 ADU for each channels. We can now deduce the calibration coefficient for the ionization channels : $\pm 55ADU \leftrightarrow 10.37keV_{ee}$.

As for the heat channel, we use the 10.37keV line forming a normal distribution visible in the ADU amplitude spectrum of the heat channel as seen in figure 1.11. The estimated center of this distribution is 1200 ADU. The calibration coefficient for the heat channel is therefore: $1200ADU \leftrightarrow 10.37keV_{ee}$.

With these calibration coefficient, it is now possible to reason with the reconstructed energy for each channels as

$$\text{Reconstructed energy [keV]} = \text{Calibration Coefficient [keV/ADU]} \times \text{Event Amplitude [ADU]}$$

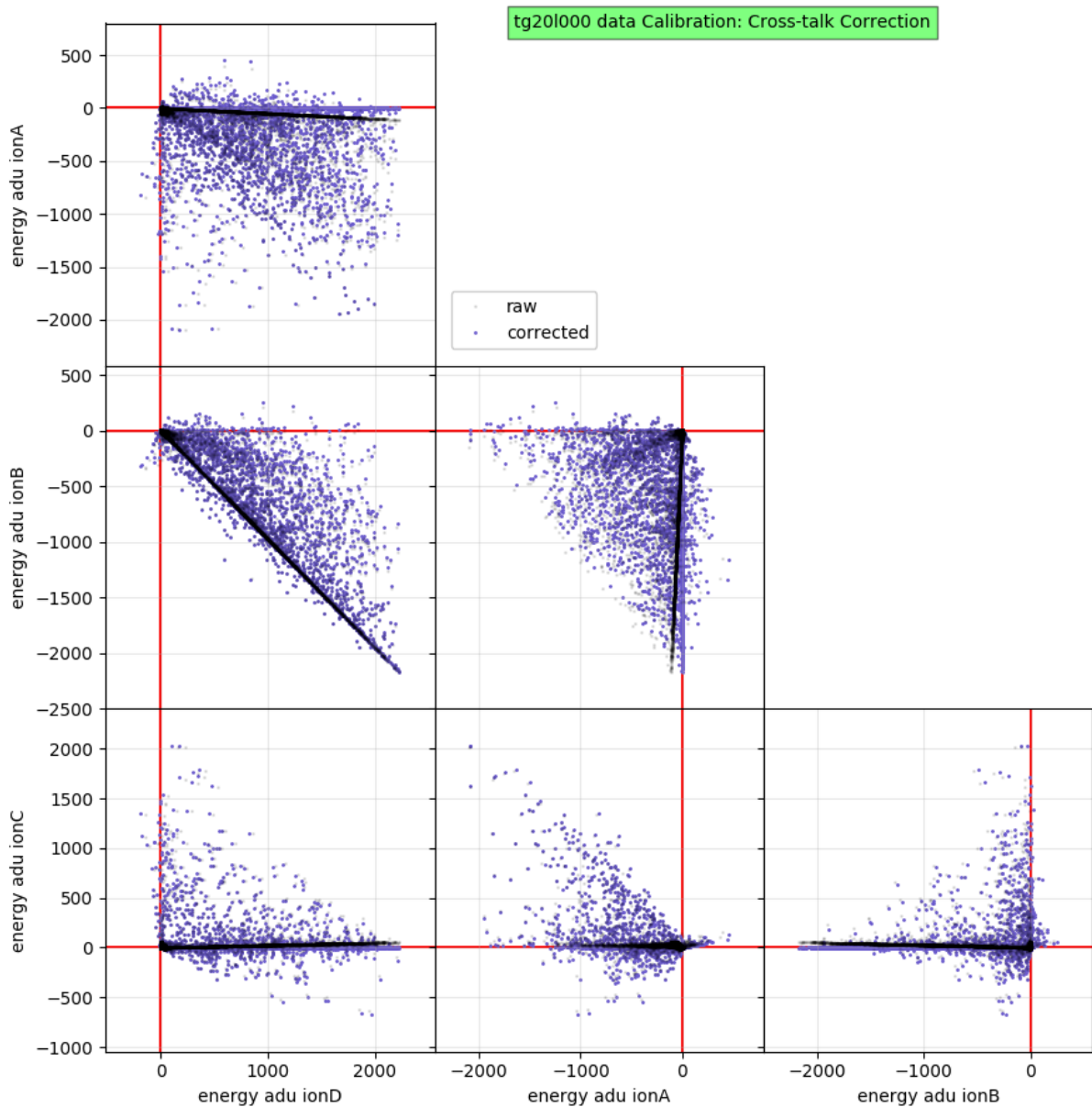


FIGURE 1.9: Corner plot of the reconstructed ionization energies of the quality events. Energies affected by the cross-talk are in grey/black, corrected energies are in blue. The x-axis and y-axis are plotted in red as visual guides.

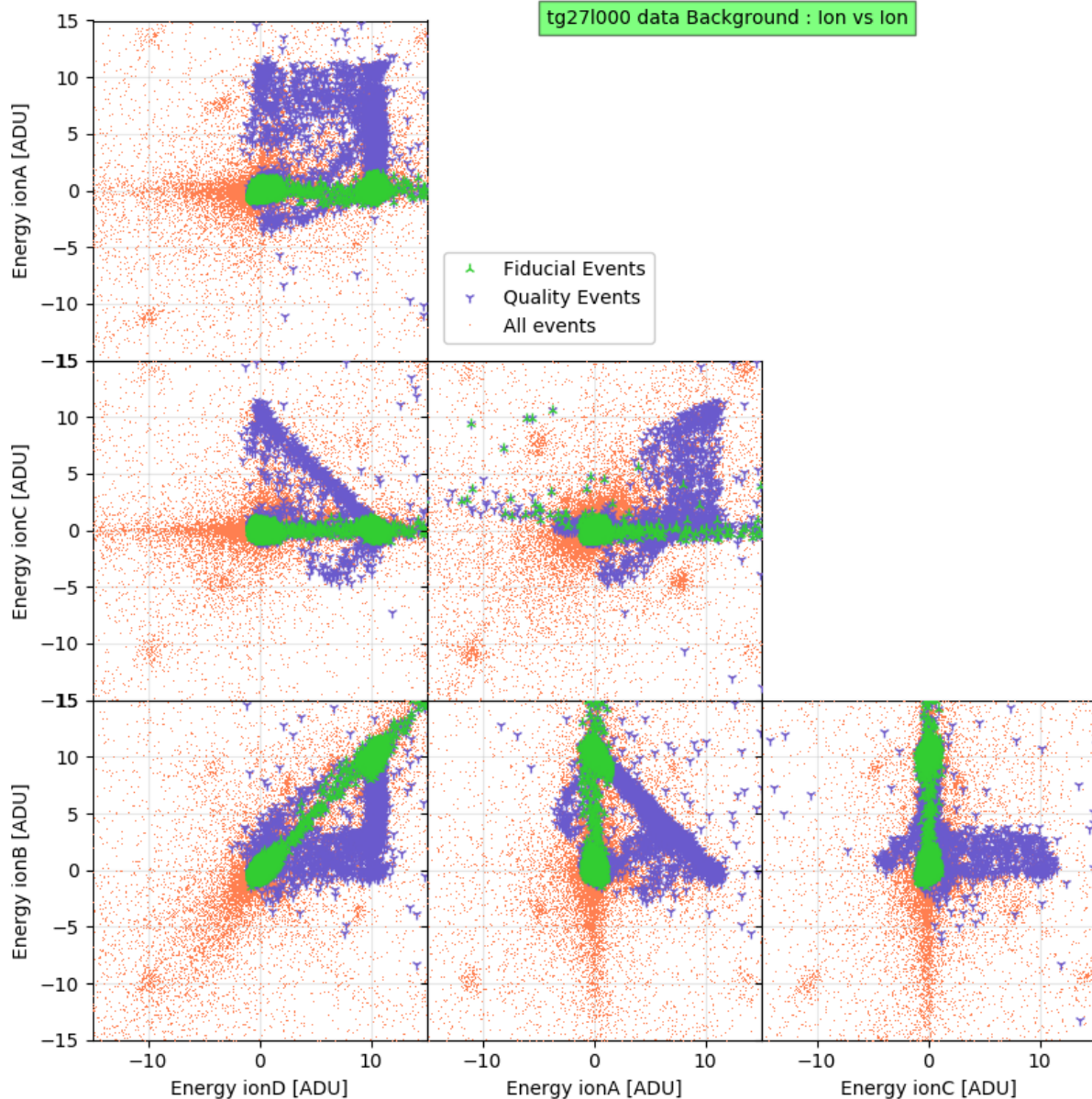


FIGURE 1.10: Corner plot of the reconstructed ionization amplitude of the quality events, zoomed on the 10.37keV calibration peak.

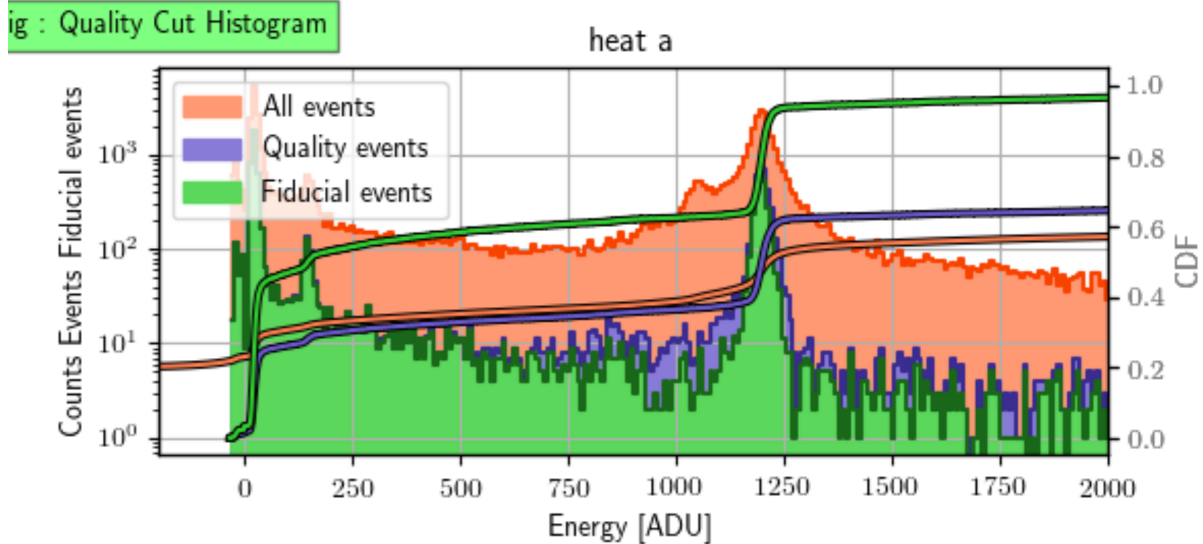


FIGURE 1.11: Heat Amplitude Spectrum for a stream. The calibration coefficient is estimated from the 10.37keV calibration peak position.

Now that the events of all the streams are calibrated, they are expressed in the same unit and can be compared. From now on, we concatenate the calibrated streams and consider all the events for the Background and the Calibration configurations.

1.8 Charge conservation cut

to be corrected vvv Even with the bulk cut, some events might still have charge collection issue. Drifting charges can be trapped in the germanium and may not end up being collected. One way to discard such events is to consider the "Charge Conservation" quantity, defined as:

$$\mathcal{C.C.} = \frac{-A - B + C + D}{2} \quad (1.6)$$

As a recoil produces electron-hole pairs, the charge of the drifting particles in the crystal should be zero as well as the total collected charges (considering their complete collection). This is characterized by a normal distribution of the $\mathcal{C.C.}$ around zero with an STD depending on the RMS resolution of the ionization channels. Events with an incomplete charge collection would stand out of this gaussian profile and can be discarded. As a result, we define the event passing this "Charge conservation cut" with a $\mathcal{C.C.}$ lower than two times the RMS resolution for the considered heat energy. This cut is represented in the figure 1.12.

As the RMS resolution depends on the energy associated to the event, it is once more necessary to model it with a linear law:

$$\sigma_{\mathcal{C.C.}}(E_{heat}) = a + b * E_{heat} \quad (1.7)$$

with the coefficient a and b coming from the estimation of the RMS resolution at 0keV (noise blob) and 10.37keV (calibration peak) (precision necessary here).

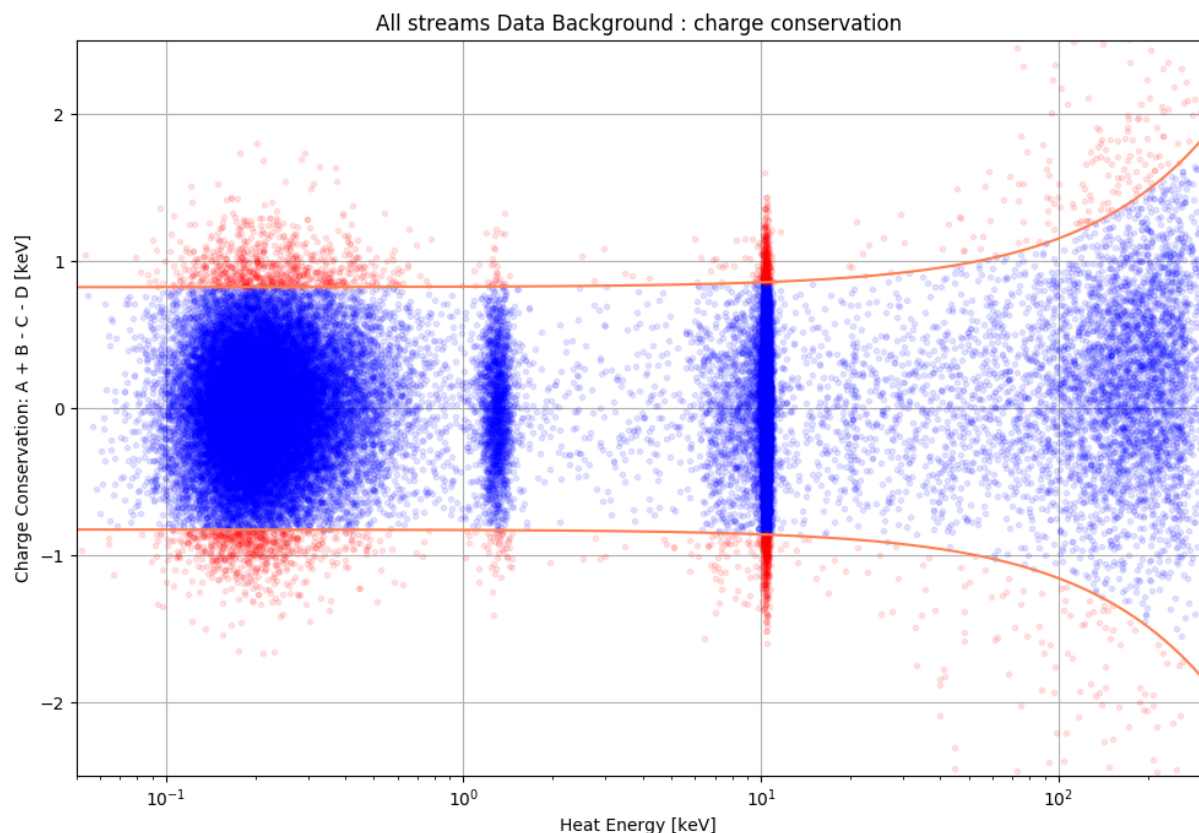


FIGURE 1.12: "Charge conservation" quantity as a function of the heat energy for the bulk quality events of the Background configuration. Passing events are in blue while discarded events are in red.

1.9 Fiducial Cut

Referring to the streamlines of the electric field in the crystal of RED80 (see Figure ??), we expect some region of the crystal with a specific drifting behavior. Represented in the Figure 1.2b, we have:

- the Bulk region, where the charge will drift towards the collect electrodes B and D,
- the Guard region, where the charge will be collected by the surface electrodes A and C,
- the Corner regions, where and , we expect the charges to recombine on place of the recoil because of the very weak electric field or become trapped on the surface by drifting along the streamlines exiting the crystal.

Surface regions are always hazardous for charge collection. Indeed, EDELWEISS has a knowledge (ref necessary) of charges drifting close to the surface devoid of electrodes being easily trapped and not being collected. This behavior is degrading the ionization signal leading to a recoil with reduced quenching factor. This means that electronic recoils happening near the surface could be reconstructed with a lower quenching and be identified as nuclear recoils. The major source of such surface recoil are the β radiation induced by the natural radioactivity interacting in the first μm of the germanium crystal (ref edelweiss necessary). Thus, we want to discard any event that may be induced by a surface recoil. When interacting on the lateral surface of the germanium crystal, this events should be collected by the guard electrodes A and C. Referring to the scheme 1.2b, the objective of the "Fiducial cut" is to discard events from the Surface zones and Corners, and keep the events induced by recoil in the bulk region of the crystal. This Fiducial cut is applied by considering the reconstructed ionization energy of the events as represented in the figure 1.13.

The Fiducial cut identifies events of the bulk region as events which did not deposited any signal on the guard electrodes A and C, with a tolerance of two $\sigma^{A,C}$ (baseline). For the bulk events, this conditions is expressed as:

$$\text{mathmathmath for bulkevents} \quad (1.8)$$

In a similar manner, we can also define the guard events with no signal on the collect electrodes B and D with a tolerance of two $\sigma^{B,D}$ (baseline). This condition then is written:

$$\text{mathmathmath for guardevents} \quad (1.9)$$

NOW, ITS GIBBERISH TIME !(yay, but to be modified) This "Bulk cut" will discard any event with a reconstructed energy on the guard electrodes A and C which is greater than two times the RMS resolution. For this purpose, it is useful to define the reconstructed total ionization energy:

$$E_{ion.,total} = \frac{A + B + C + D}{2} \quad (1.10)$$

As the RMS resolution σ_i of given channel i depends on the total ionization energy deposited in the crystal, it is modeled by a power law:

$$\sigma_i(E_{i,total}) = \sqrt{(\sigma_i(0\text{keV}))^2 + (\alpha E_{ion.,total})^2} \quad \text{with} \quad \alpha = \frac{\sqrt{\sigma_i(10.37\text{keV})^2 - \sigma_i(0\text{keV})^2}}{10.37\text{keV}} \quad (1.11)$$

In this equation, the baseline resolution $\sigma_i(0\text{keV})$ is estimated with the standard deviation of the noise blob while the resolution $\sigma_i(10.37\text{keV})$ is estimated with the standard deviation of the events associated to the germanium calibration peak. **END of GIBBERISH, i think**

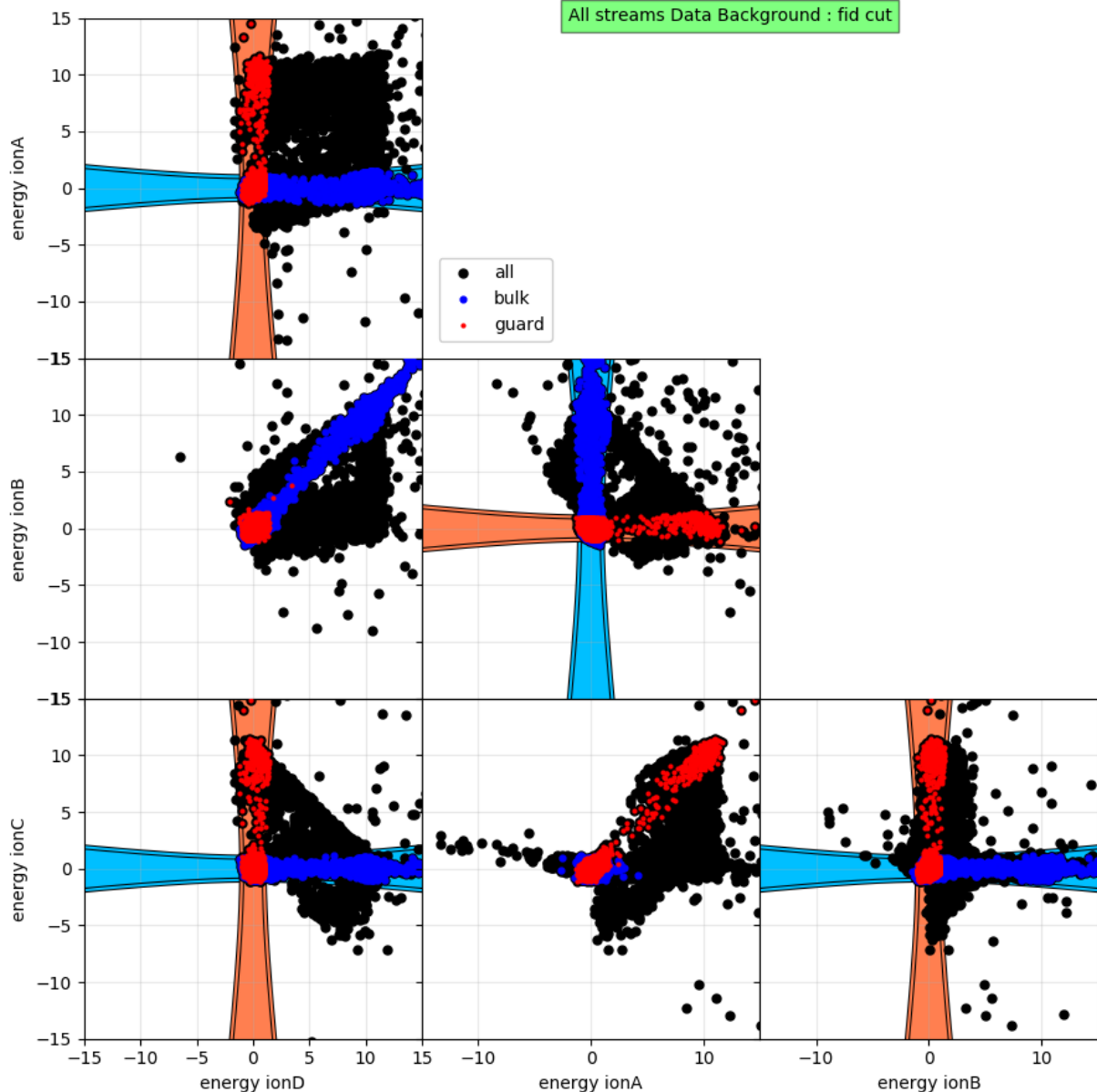


FIGURE 1.13: Corner plot of the reconstructed ionization energy for each electrodes for the quality events of the Background configurations. The energy thresholds for the cuts as well as the passing events are highlighted in the associated colors: blue for "bulk cut" and red for "guard cut".

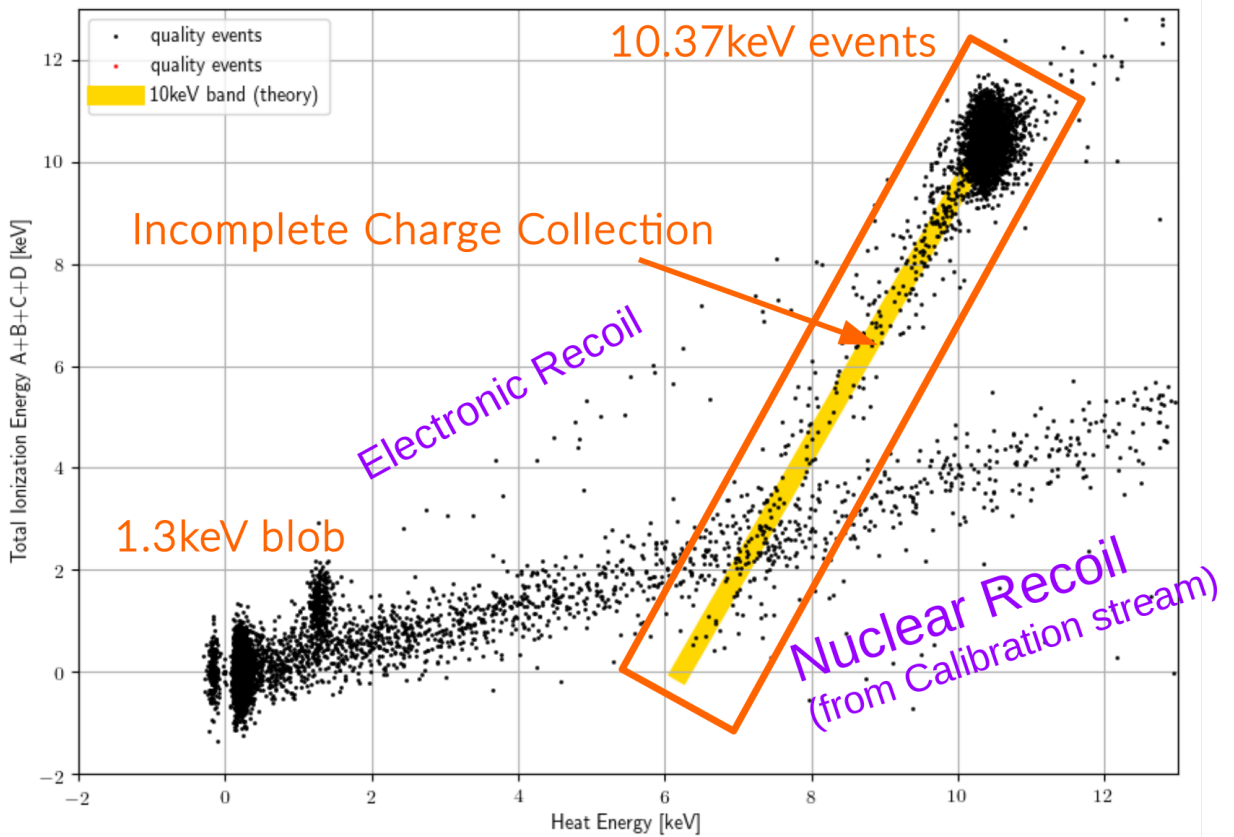


FIGURE 1.14: Reconstructed Ionization Energy in function of the Reconstructed Heat Energy, for the quality events of the Calibration configuration. The plot is zoomed up to 12keV for an easier view of the calibration peaks.

We have discarded the events with a possible bad energy reconstruction energy and calibrated the remaining ones. The experimental signal obtained with the heat and ionization channels were reconstructed into heat energy E_{heat} and total ionization energy E_{ion} . The figure ?? shows the scatter plot of these two values for the events of the Calibration configuration.

We recognize the noise blob near the origin corresponding to recoils of very low energy and triggering noise windows. Expanding from this noise blob, we note two bands. The electronic recoil band corresponds to events depositing the same energy in the ionization channel and the heat energy channel (both in keVee). They are characterized by a quenching factor of 1. As a matter of fact, the gamma recoil of 1.3keV and 10.37keV coming from the calibration peaks of the germanium belongs to this band. Any event below this band deposited less energy in the ionization channel than in the heat channel, and therefore possess a quenching factor inferior to one. We see that the population blob associated to the 10.37keV is smeared to lower quenching factor. This is due to events of the calibration peaks with incomplete charge collection. We note that this population is following a linear trend, which can be explained by an incomplete Luke-Neganov Boost of the heat channel according to the equation:

$$E_{heat} = 6\text{keVee} + \epsilon \frac{2V}{\epsilon_{Ge}} E_{ion}. \quad (1.12)$$

The other major population of events below the electronic recoil band counts a lot of events in the case of the Calibration configuration. This hints that this band corresponds to the nuclear recoil induced by the AmBe neutron source. The presence of the two bands in this plot demonstrate the discriminating ability of the associated heat and ionization channels. Note that, although

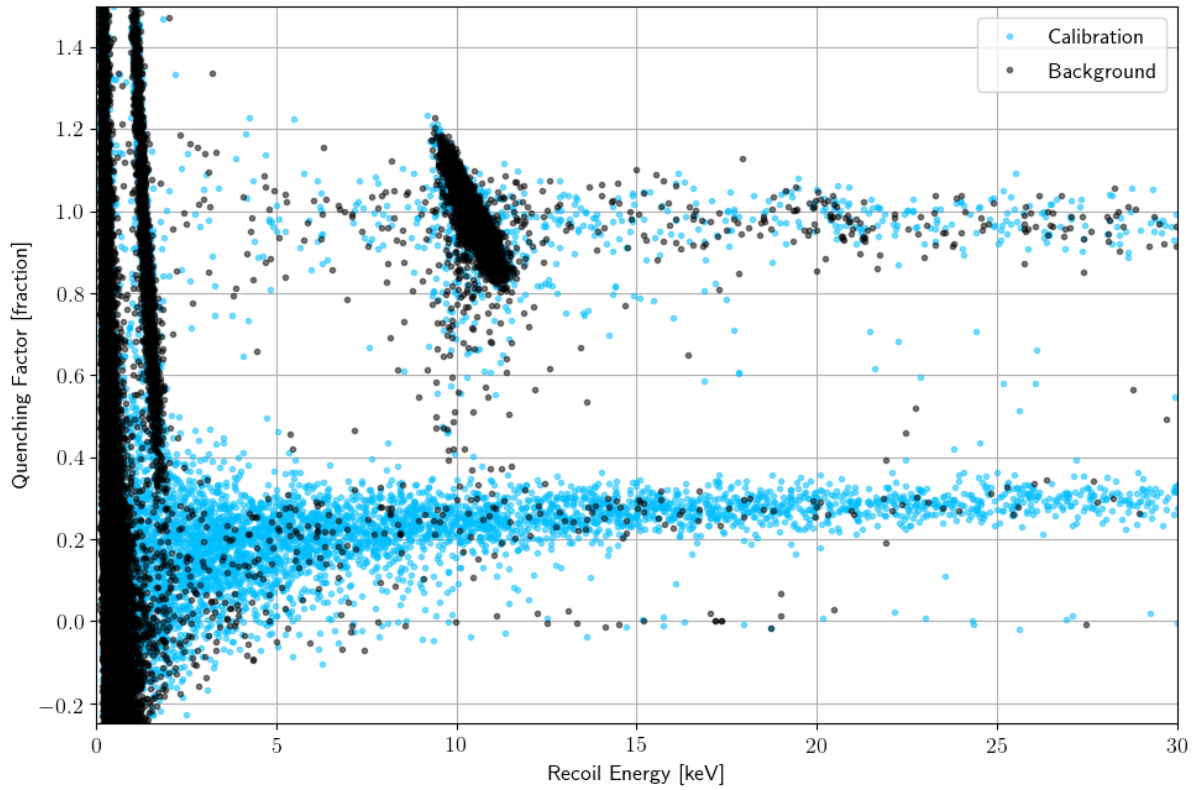


FIGURE 1.15: Quenching value Q for each quality events of the Background (black) and Calibration (blue) configurations in function of their recoil energy E_R .

the bands are well separated at high energy, they are merging at low energy due to their width which is fixed by the energy resolution of the heat and ionization channel.

Another way to represent the discrimination between the electronic and the nuclear recoil is to compute the recoil energy E_R and the quenching factor Q for each event:

$$E_{NL} = \frac{V}{\epsilon} (E_{ion,???} - E_{heat}) \quad (1.13)$$

$$E_R = E_{heat} - E_{NL} = E_{heat} \left(1 + \frac{V}{\epsilon} \right) - E_{ion,???} \frac{V}{\epsilon} \quad (1.14)$$

$$Q = \frac{E_{ion,???}}{E_R} \quad (1.15)$$

with E_{NL} being the heat energy boost coming from the Neganov-Luke effect [2]. The recoil energy E_R is expressed in the usual keV energy unit, as the Luke-Neganov Boost depending on the type of recoil was substracted from the heat energy. The Quenching factor is unitless. The figure 1.15 show, for each configuration, the quenching factor as a function of the recoil energy.

We recognize the electronic band, centered around $Q = 1$ and the nuclear recoil band with $Q < 0.4$. We also note some inter-band events like the smearing of the 10.37keV events hinting at the incomplete charge collection.

However, there are some interesting events with a quenching factor $Q = 0$ which are known as "Heat-only" events. This population is infamously known in domains in the EDELWEISS experiment [ref?] and CRESST [ref?]. This population could correspond to events with no charge collection, but this is not compatible with the lower count of inter-band events with an incomplete charge collection. An other and more realistic explanation would be the existence of energy

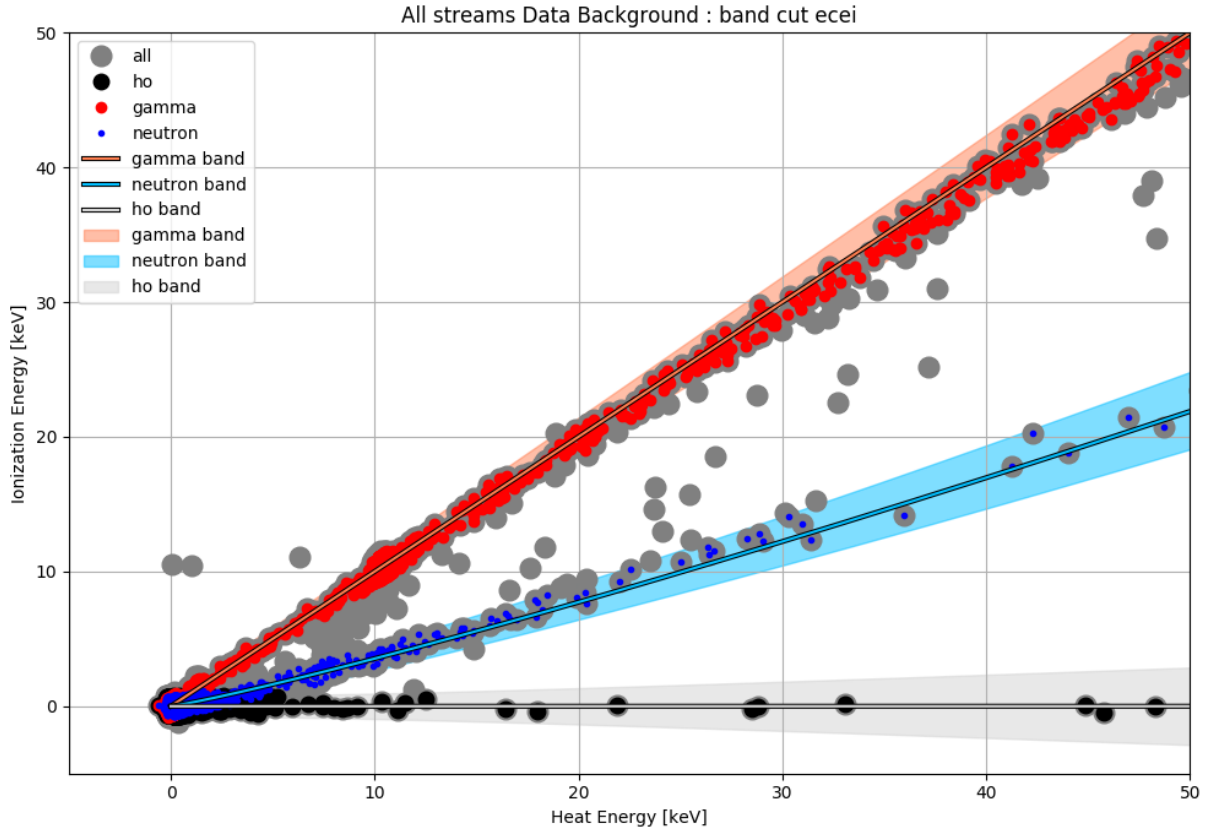


FIGURE 1.16: Band cut representation on the graph of Ionization energy vs Heat energy.

deposit in the crystal without ionization. The source of this Heat-only event is still under investigation [ref?].

The merging phenomenon of the bands at low energy is also more visible in this graph with the change of variable. We can even visually witness that the lower part of the 1.3keV event blob is leaking into the higher part of the nuclear band.

1.10 Band cut

With the obtainment of well reconstructed events, it is now time to count the events corresponding to electronic and nuclear recoils. The events will be allocated into different population based on their quenching factor and the resolution of the heat and ionization channel at the considered energies. This "band cuts" are represented on the figure 1.16 with ionization and heat energies and on the figure 1.17 by reasoning on the quenching factor and the recoil energy.

Paragraph on the quenching, recoil energy here, but will surely be moved in a previous chapter !

Electronic recoils are characterized by a quenching factor $Q_{ER} = 1$. Nuclear recoil are associated to lower quenching factor depending on the recoil energy E_R and the material of the absorber. According to the literature [Lindhard ref], with an atomic number of $Z = 32$ and an average number of nucleons of $A = 72.63$, the quenching factor of a nuclear recoil in a pure-germanium crystal is expressed as:

$$Q_{NR}(E_R) = \frac{kg(E_R)}{1 + kg(E_R)} \quad (1.16)$$

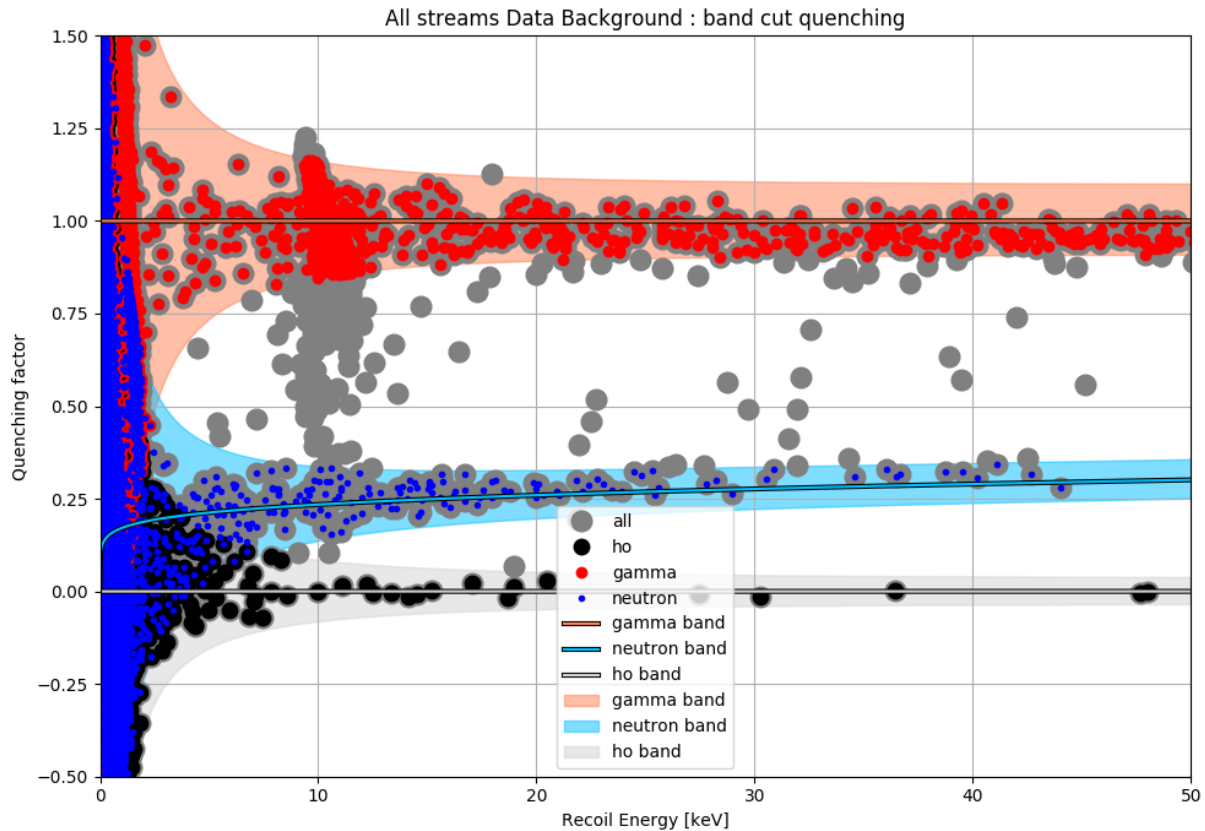


FIGURE 1.17: Band cut representation on the graph of Quenching vs Recoil Energy.

with the k, g terms calculated as:

$$k = 0.133 Z^{\frac{2}{3}} A^{-\frac{1}{2}} \quad (1.17)$$

$$\epsilon(E_R) = 11.5 E_R Z^{-\frac{7}{3}} \quad (1.18)$$

$$g(E_R) = 3\epsilon(E_R)^{0.15} + 0.7\epsilon(E_R)^{0.6} + \epsilon(E_R) \quad (1.19)$$

The heat-only event show a null quenching $Q_{HO} = 0$.

These constraints on the quenching factor are translated in term of ionization and heat energy with the change of variables induced by eq 1.13. For the electronic recoil, the ionization and heat energies follow:

$$E_{heat,ER} = E_R \frac{1 + Q_{ER} \frac{V}{3}}{1 + \frac{V}{3}} = E_R \quad (1.20)$$

$$E_{ion.,ER} = E_R Q_{ER} = E_R \quad (1.21)$$

The heat and ionization energy are theoretically equals. For the neutron recoil, the energies follow:

$$E_{heat,NR} = E_R \frac{1 + Q_{NR}(E_R) \frac{V}{3}}{1 + \frac{V}{3}} \quad (1.22)$$

$$E_{ion.,NR} = E_R Q_{NR}(E_R) \quad (1.23)$$

As for the heat-only events, the energies are modeled as:

$$E_{heat,HO} = E_R \frac{1 + Q_{HO}(E_R) \frac{V}{3}}{1 + \frac{V}{3}} = E_R \frac{1}{1 + \frac{V}{3}} \quad (1.24)$$

$$E_{ion.,HO} = E_R Q_{HO}(E_R) = 0 \quad (1.25)$$

End of quenching paragraph to be moved.

An experimental event is allocated to the electronic recoil "ER" band if its ionization energy $E_{ion.,exp}$ and heat energy $E_{heat,exp}$ follow the energy function associated to the ER recoil 1.20 with a tolerance of two times the RMS resolution of the ionization energy at the considered heat energy, $\sigma_{ion}(E_{heat,exp})$. This condition to be satisfied is mathematically written as:

$$|E_{ion.,exp} - E_{ion,ER}(E_{heat,exp})| < 2 \times \sigma_{ion}(E_{heat,exp}) \quad (1.26)$$

Taking into account the equality of the heat and ionization energy in 1.20, this condition is also written as:

$$|E_{ion.,exp} - E_{heat,exp}| < 2 \times \sigma_{ion}(E_{heat,exp}) \quad (1.27)$$

Concerning the allocation in the neutron recoil "NR" band, the heat and ionization energies should now follow the functions associated to the neutron recoil 1.22. The tolerance is still fixed to two times the RMS resolution $\sigma_{ion}(E_{heat,exp})$. The condition now is expressed as:

$$|E_{ion.,exp} - E_{ion,NR}(E_{heat,exp})| < 2 \times \sigma_{ion}(E_{heat,exp}) \quad (1.28)$$

One should note that according to the expressions 1.22, their is no analytical expression of the ionization energy $E_{ion,NR}$ as a function of the heat energy. To bypass this issue, $E_{ion,NR}$ is computed over a fine array of heat energy between 0keV and 50keV. The term $E_{ion,NR}(E_{heat,exp})$ is therefore obtained by linear interpolation.

As for the allocation to the heat-only "HO" band, we use the modelization of the heat-only event energies in equations 1.24 to define the condition:

$$|E_{ion.,exp} - E_{ion,HO}(E_{heat,exp})| < 2 \times \sigma_{ion}(E_{heat,exp}) \quad (1.29)$$

which is simplified to:

$$|E_{ion.,exp}| < 2 \times \sigma_{ion}(E_{heat,exp}) \quad (1.30)$$

The ER, NR and HO band defined by the three previous conditions 1.27, 1.28 and 1.30 respectively are represented on the figure 1.16 along with the experimental events passing the quality cuts. With the change of variable 1.13, the ER, NR and HO bands are also defined in terms of quenching factor and recoil energy in figure 1.17. It is now possible to obtain a raw recoil energy spectrum of the different bands by counting the number of events in each energy bins. These histograms are presented in figure 1.18.

We can note some usual features in this histogram like the noise blob at the lowest energies, the 1.3keV events and the 10.37keV of the calibration peaks. As before, we see that from 6keV and below, the different bands are merging into each other. The lower parts of the 1.3keV and 10.37keV population of the calibration peaks are even counted in the NR and HO band ! This contamination between the bands is harmful for an unbiased counting of the events in each bands. Moreover, the experimental events presented in the figures were the one passing the quality cuts presented previously. Even though this cuts were vital to prune the data from ill-reconstructed events, they effectively reduced the number of events in the ER, NR and HO bands, which are therefore underestimating the initial number of recoils having happened.

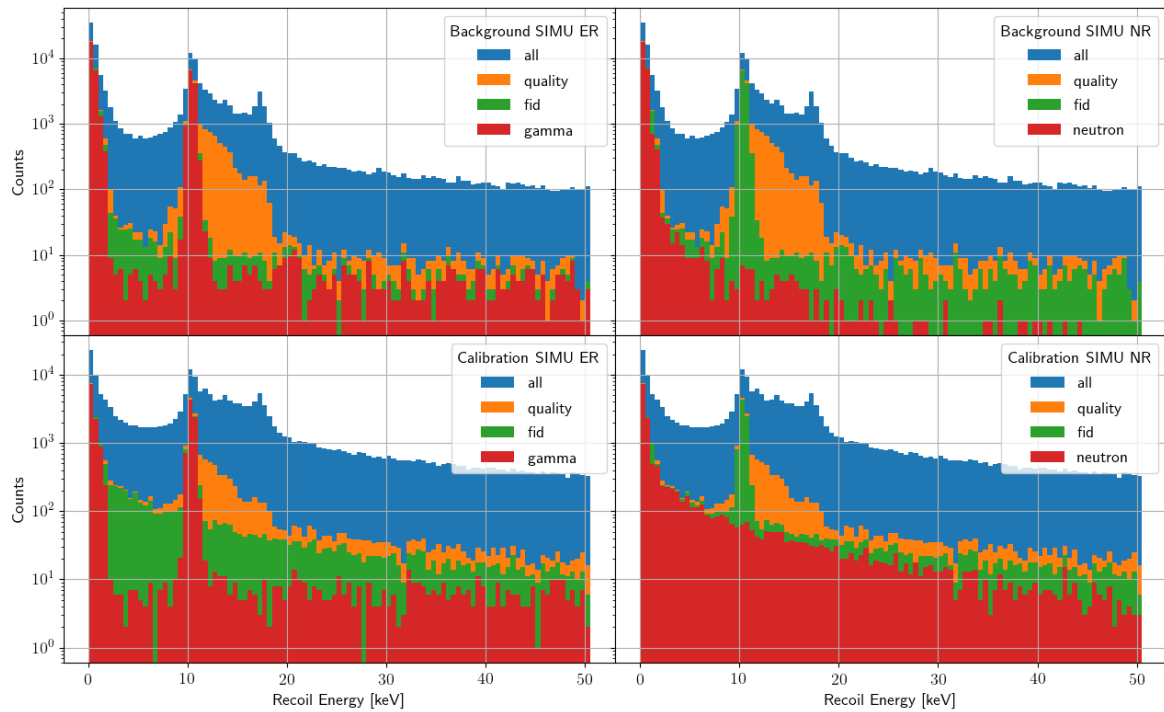


FIGURE 1.18: Histogram of the event allocated to the ER, NR and HO bands in function of their recoil energy.

1.11 Pulse simulation

In order to estimate the true ER, NR and HO background, it is necessary to correct the raw histograms 1.18 from the following bias:

- the efficiency of the quality cuts, to take into account all the events which did not pass the quality cuts
- the cross-band contamination, particularly at the lowest energy when the bands are merging

In this analysis, we choose to use a method called "Pulse Simulation" to estimate these bias and correct for the livetime.

This method aims at simulating signals (aka pulses) of ER and NR recoil with known recoil energy and injecting them into the experimental stream. Thus, this technique is only valid when the whole stream of data is saved.

The simulation of a signal comes from a bank of well characterized events. This bank is built with a selected population of 10.37keV event from the associated calibration peak passing the quality cuts as represented in the figure 1.14. These selected events comes from gamma recoils with a known recoil energy. Although most of these events present a complete charge collection associated with a quenching $Q_{ER} = 1$, some are subjects to incomplete charge collection (and still taken into account ??? are discarded ??? idk).

Once the bank of 10.37keV events is formed, we proceed with the the simulation of events coming from ER and NR recoil and with the wanted recoil energy. We fix the recoil energy of a simulated event by scaling the signal of the 10.37keV event from the bank. Simulating event coming from electronic recoil is straightforward as the 10.37keV event of the bank are already produced by gamma recoils. As for the simulation of events coming from nuclear recoil, the

ionization and heat energies should be corrected to present a quenching calculated from the Linhard formula in equation 1.16.

In this analysis, four different population of events were simulated:

- 10.37keV line ER events: the most straightforward simulation as these simulated corresponds to the raw selected events of the bank.
- 1.3keV line ER events: simply rescaling the bank of events provides this simulated population corresponding to the second calibration peak of the germanium.
- [0 – 50]keV flat ER events: this uniform distribution in recoil energy is obtained by rescaling the bank of events by random factors.
- [0 – 50]keV flat NR events: as before, this is a uniform distribution in recoil energy and corrected in heat and ionization energy to present an appropriate quenching factor Q_{NR} .

The pulse simulation continues with the injection of these simulated population into the saved streams. This means taking one event of a population, and adding it to stream at a random known time t_0 . In order to keep this probing technique from altering too much the characteristics of the analysis, it is decided to inject a maximum of 60(?) pulses per hour of streams. This process is repeated multiples times with different t_0 and for the four simulated population independently.

This paragraph is no longer relevant because the pulse simulation is analytical and thus injects perfect theoretical pulses into the the stream. The selected quality 10.37keV events are fitted with a 3exponential model. Therefore, no additional noise is injected into the stream. This is easy to check with a chi2 heat vs energy graph, where the real pulse will show a diverging band while the simulated should remain constant. There is however a added deviation on the 10.37keV resolution (this phenomenon is negligible as the heat resolution at 10.37kev is much greater than the heat resolution of the baseline) An important remark is to be made here concerning the signal noise injected in the streams along with the simulated pulses. The 10.37keV events composing the bank of events and used for the creation of the simulated population are real events from the streams affected a signal noise. By adding simulated pulses to the streams, we are effectively adding the noise of the simulated pulse and the noise of the stream. This means that all the pulses that are injected into the streams are by construction noisier than real pulses. While the effect of this phenomenon is negligible at low energies as the 10.37kev and its associated noise were scaled down, for higher energies this additional noise might result in a worse energy reconstruction than real pulses as well as lead to a discarding by the χ^2 cut. As a concrete example, an injected pulse of the "10.37keV line ER" population should be affected by a noise PSD with a factor $\sqrt{2}$ higher than the noise PSD of a real 10.37keV pulses of the stream. This will result in a biased χ^2 value for the simulated pulse, sampled from a χ^2 distribution of mean $\sqrt{2}N$ rather than \sqrt{N} . Hopefully, the χ^2 cut of this analysis (presented in 1.5) are large enough to alleviate this effect. As for the energy reconstruction, the bias should be compensated by the energy resolution of the sensors. As we know that the pulse simulation accuracy is reduced for high energies, the energy range chosen for the simulation is set to be [0-50] keV. This limited energy range should pose no threat to the measurement of the neutron background as it is expected to be observed at low energy (thanks to kinematics considerations).

Having considered the existence of this added noise, we can considered that the simulated pulse are excellent facsimiles of the real pulses, especially at the lowest energies, with the major advantages than we know their input recoil energy E_R^{input} , their injection time t_0^{input} and their quenching Q_{ER} or $Q_{NR}(E_R^{input})$ (depending on the simulated population they belong to).

1.12 Trigger cut

this explanation definitively needs a plot to explanation all the different cases and the different t0, else this will be too much confusing :

Just as in the previous section 1.3, the newly created streams with injected pulses are processed using the same pipeline and information on the triggering time windows are saved. As what is interesting us in this streams are the injected pulses, we are focusing on the triggering events. The objective is this section is to decide whether a simulated event injected at t_0^{input} has properly triggered or not. On the one hand, we should discard "non-triggering" simulated event where:

- the simulated pulse with a low energy could not have reach the trigger threshold, and the an earlier or later real triggering pulse was selected as closest to the injection time t_0^{input}
- a simulated pulse could have been injected near a real pulse of higher energy. As both the simulated and the real pulses are triggering and are close in time, only the real one with the highest reconstructed energy is triggering.

A maximum tolerance of 5ms between the injection time of a simulated pulse t_0^{input} and the timestamp of the closest triggering event t_0 was found optimal (cf fig + paragraph on this study) to ensure that the triggering pulses are in fact corresponding to simulated pulses. On the other hand, a triggering simulated event could also have been injected exactly at the same time as a real pulse of the stream, this occurrence is called a "pile-up". The resulting signal is the addition of a real and the injected pulse which will bias the energy reconstruction. A minimum time of 5ms between the timestamp of the closest triggering event t_0^{input} (extracted from the stream with injected simulated pulses) and the timestamp of the closest triggering real pulse t_0^{data} (extracted from the original stream) was similarly chosen to discard any pile-up event. By combining this two condition ensuring a proper triggering of the simulated event, we can define the "trigger cut" condition:

$$\begin{cases} |t_0^{input} - t_0| \leq 5\text{ms} \\ |t_0 - t_0^{data}| \geq 5\text{ms} \end{cases} \quad (1.31)$$

Triggering event of timestamp t_0 closest to a t_0^{input} satisfying this condition are considered as having properly triggered.

nuance nece It is important to note that this trigger cut is specific to simulated pulses. In order to reproduce such a study with real pulses can only be done if we know the exact time of the energy deposit in the crystal. Access to this piece of information is impossible in this work using either an AmBe neutron source or the gamma calibration peak of the germanium as both this source are based on the intrinsically stochastic process of radioactive decay. However, the use of controlled source of particles could be envisioned:

- facing the germanium crystal inside the cryostat, an optical fiber linked to a pulsing LED could be used as a repetitive source of electronic recoil.
- outside of the cryostat, a pulsed neutron source would be overkill (or would it ? idk just thinking here)

Now that we have selected the simulated pulses which properly triggered, the entire analysis chain of this very chapter described until now is applied to these events. The triggering simulated events population is pruned of the reconstruction biased with the quality cuts and are then allocated to the ER, NR and HO bands (see Figure 1.19)

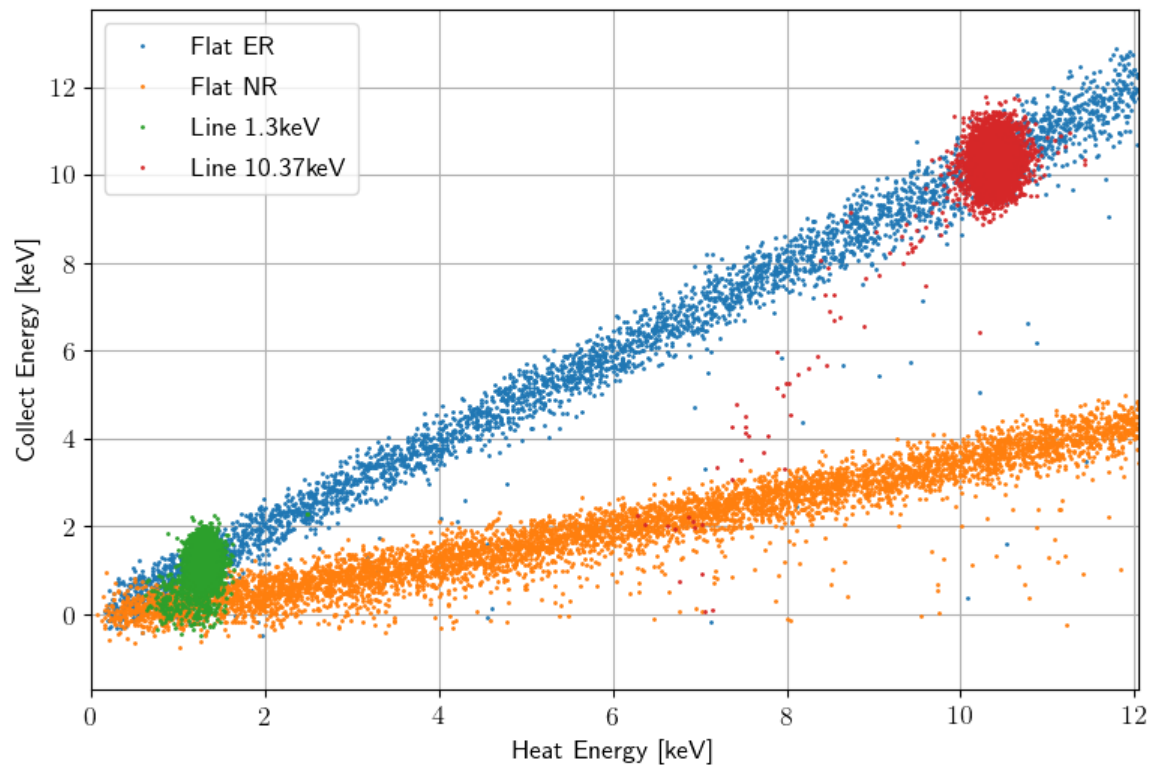


FIGURE 1.19: Ionization energy as a function of heat energy for the four population of simulated events. Represented events passed the quality cuts and are allocated to the ER, NR and HO bands.

1.13 Band Contamination Correction

DISCLAIMER: Proper paragraph with mathematical expression coming later. For the moment, just an idea dump

The objective of this section is to correct the histograms of the Figure 1.18 from the leakage of the band events into others. A rigorous but time-consuming method would be the use of a likelihood modeling the distribution of the ER, NR and HO events in term of ionization and heat energy. However, given the short time frame induced by the advancement of the RICOCHET experiment proposal, it was decided to correct the measurements using quicker binned statistics. While this latter method effectiveness is heavily affected by the choice of the binning, the induced bias are small and constitute a very good approximation to the more rigorous likelihood method.

The binning chosen for the rest of the analysis and the presentation of the results is logarithmic and scales with the recoil energy resolution. The logarithmic profile (as well as the linear profile) is convenient for the visualization of energy spectrum and can be easily compared to the results of neutron background simulation obtained with GEANT4 (ref necessary). The size of the bins is set to scale with the recoil energy resolution as to properly analyze, correct and present the event counts at each energy scale. The bins are set to start at the inferior energy threshold of the analysis, which corresponds to the energy threshold of the trigger $E_{inf} = 200\text{eV}$? in the pre-processing step described in section 1.3. The end of the binning corresponds to the superior energy limit of $E_{sup} = 50\text{keV}$ imposed by the pulse simulation.

Insert mathematical definition of the binning here. With a number N of bins of equal widths in logarithmic scale W of the base b , the following equations holds:

$$\log_b E_{sup} - \log_b E_{inf} = N \times W \Leftrightarrow W = \log_b \left(\left(\frac{E_{sup}}{E_{inf}} \right)^{\frac{1}{N}} \right) \quad (1.32)$$

Now, if we want to properly study the features of the energy spectrum at different energy scales, mainly the 1.3keV and the 10.37keV, we should consider a bin width of a tenth of the recoil energy resolution $\sigma_{E_R}(E_R)$. Thus, these constraints are expressed as:

$$\begin{cases} \sigma_{E_R}(1.3\text{keV})/10 &= \text{Bin width at } 1.3\text{keV} = 1.3\text{keV} (b^W - 1) = 1.3\text{keV} \left(\left(\frac{E_{sup}}{E_{inf}} \right)^{\frac{1}{N}} - 1 \right) \\ \sigma_{E_R}(10.37\text{keV})/10 &= \text{Bin width at } 10.37\text{keV} = 10.37\text{keV} (b^W - 1) \end{cases} \quad (1.33)$$

ANYWAY, let's continue ... only N can fix the bin width at a single energy. Impossible to have the bin width corresponds for two points... welp, logarithmic scale for you >:(better to have a power law or something like that to have a little more control on what is th transform and adjust just like i want...

It is important to keep in mind that the contamination correction is possible because of the knowledge of the electronic recoil background (ref necessary). Indeed, this background should be constituted by events coming from the calibration peaks of the germanium and from Compton scattering processes. The calibration peaks forms components of normal distributions centered at 1.3keV and 10.37keV, of unknown amplitude $A_{1.3\text{keV}, 10.37\text{keV}}$ and scale $\sigma_{1.3\text{keV}, 10.37\text{keV}}$, while the Compton background is modeled as a uniform distribution of unknown amplitude $A_{Compton}$. Determining these unknown parameters amounts to measuring the electronic recoil background. Knowing the amplitude of each components of the electronic background, we also have access the fraction of leakage of each components into the NR and HO bands. Subtracting these fraction from the NR and HO band yields corrected energy spectra.

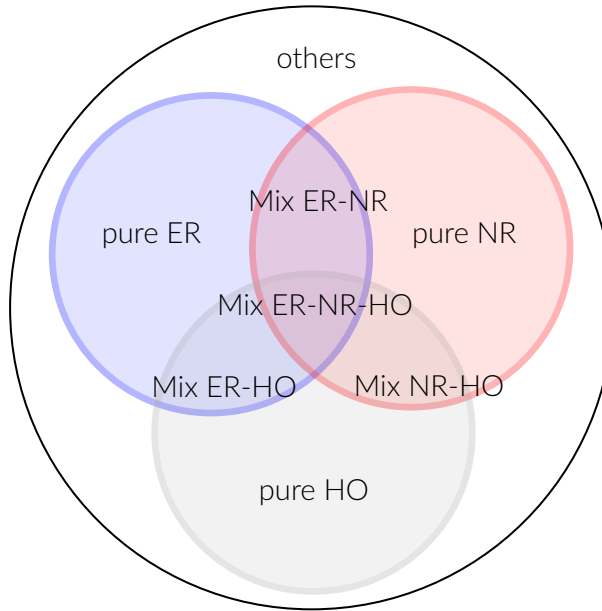


FIGURE 1.20: Venn Diagram of the sets of events in respect to the ER, NR and HO cut.

With simulated events induced by ER or NR recoil, it is now possible to estimate the efficiency and the contamination of the ER, NR and HO bands. As presented in the Figure 1.19, we can count the number of simulated event of a considered population allocated to the different bands. For each population of simulated events, several sets of events are defined according to satisfaction of the band conditions as presented in Figure 1.20.

The simulated events are separated in eight non-intersecting sets:

- the "Pure ER" set, for events allocated to the ER band only.
- the "Pure NR" set, for events allocated to the NR band only.
- the "Pure HO" set, for the events allocated to the HO band only.
- the "Mixed ER-NR" set, for the events allocated to the ER and NR band.
- the "Mixed ER-HO" set, for the events allocated to the ER and HO band.
- the "Mixed ER-HO" set, for the events allocated to the ER and HO band.
- the "Mixed ER-NR-HO" set, for the events allocated to the ER, NR and HO band.
- the "Others" set, for the events not allocated to any band.

Event though these sets hold for every recoil energy, the mixed sets are mainly populated by events of low energy where the bands are merging. That is why the 1.3keV calibration events compose the main component to be substracted from the NR band.

First, we should know what amount of events in each bins of the NR band corresponds to ER recoil. For this, we need to estimate the number of experimental events induced by ER recoil. This estimation is possible because we have a modelization of the ER background. Thanks to the simulated NR events, we know that the NR events leakage into the "Pure gamma" set is negligible. Thus, the set of interest for the ER background modelization fitting is the "Pure gamma" one. The figure 1.21 presents the histograms of the experimental events for the Background and the Calibration configuration. Each histogram is used to adjust the ER background modelization.

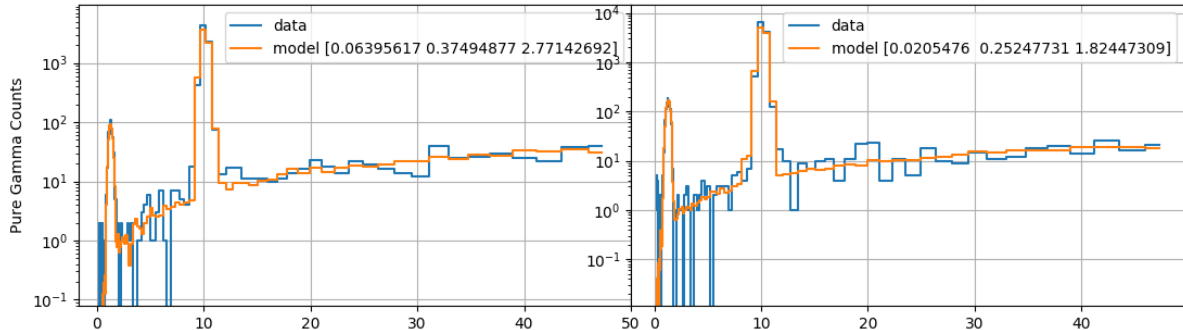


FIGURE 1.21: Histogramm of the experimental events allocated belonging to the "Pure ER" set, and fitting of this histogram with the electronic background model.

We now know the weight, and the number of events, associated to each components of the ER background modelization. Thus, we have now access to the number of simulated events of the 1.3keV, 10.37keV and flat ER population allocated to the NR band. These numbers are therefore subtracted from the NR band and added to the ER band. The recoil energy spectrum corresponding to the ER and NR bands are now corrected of cross-contamination for both configuration Background and Calibration.

1.14 Efficiency correction

Up until this section, the presented analysis has mainly pruned the initial experimental events with different cuts. In the end, only a fraction of all the events that did happen into the detectors did trigger, passed the cuts and are used to estimate the NR and ER background. In order to obtain the initial number of recoil in the detector it is necessary to correct the energy spectra with the efficiency of each cuts.

Not an accurate description of the cuts. Should refer to the initial recoils in the crystal. to be corrected. Maybe explain the cut before the analysis... defendable...

In the presented analysis, a cut is essentially a binary classification. This means that a cut classifies a given set of events into two groups. For example, the quality cut is a test whose objective is to discriminate the events with good energy reconstruction from others. However, all the cuts rely on estimators and are therefore prone to errors: the outcome of the cut can be different from the actual condition of an event. This leads to four possible combinations of the outcome of the cut and the actual condition which are: true passing, true discarded, false passing, false discarded. In this work, the cuts were chosen to minimize the amount of false passing events, which might otherwise lead to an incorrect estimation of the neutron background. This choice also impose a possibly high amount of false negative. The efficiency of a cut in the i -th bin is defined as:

$$Eff_i = \frac{N_i \text{ (true passing)}}{N_i \text{ (true passing)} + N_i \text{ (false discarded)}} = \frac{N_i \text{ (true passing)}}{N_i \text{ (injected pulses)}} \quad (1.34)$$

with $N(A)$ corresponding to the number of events for the one of the four combination A . The efficiency is used to correct the energy spectra and account for the false negative that were pruned from the data set. While the efficiency is not obtainable with the experimental data alone, it can be estimated with the pulse simulation. The simulated flat ER and the simulated flat NR are used to obtain the efficiency of each cut for the ER and NR energy spectrum respectively.

The figure 1.22 presents the efficiency factor of each cut for the each band and configuration. The "all" cut in this figure is plotted for reference as a cut accepting all the events (and with an efficiency of 1 by definition). The main results presented is the efficiency levels corresponding

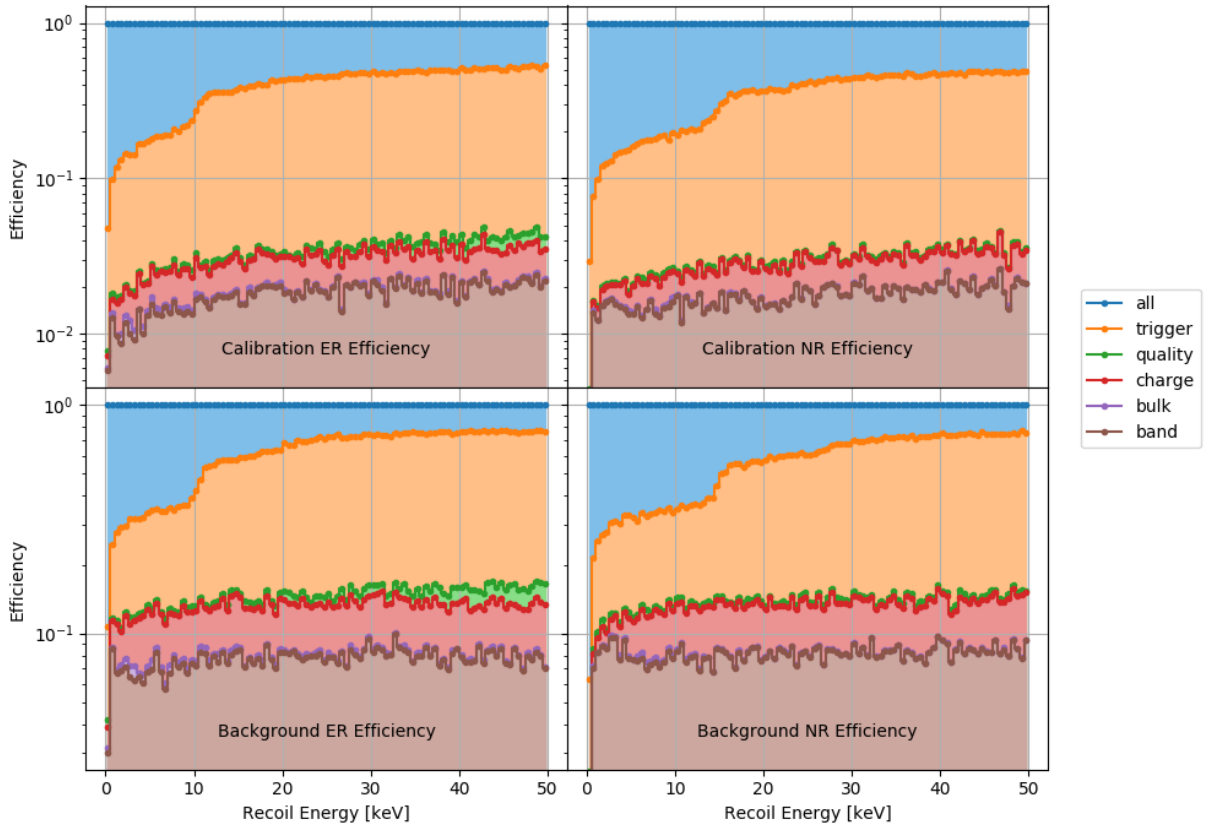


FIGURE 1.22: Efficiency of the cumulative cuts as a function of the recoil energy for the two configurations, Background and Calibration, as well as for the events of the ER and NR bands.

to the last layer of cut which directly yields the correction factor for the energy spectra. For the Calibration configuration, both the ER and NR bands show an efficiency of about 2%. For the Background configuration, both bands show an efficiency of about 8%. This means that only a few percent of the initial ER and NR recoils which did happen inside the detector induced an event that triggered and passed all the cuts. We can diagnose the successive pruning of the recoils by looking at the efficiency of the previous layers of cut.

The trigger cut, defined in section 1.12, aims at selecting the simulated events that triggered during the optimal filtering pre-processing step in section 1.3. Its efficiency is an estimation of the livetime of the detector, which is the fraction of the time that the detector was available to register an event. For each combination presented in figure 1.22, this efficiency is dropping at the lowest energies. This can be explained by the screening of the low energy by events of higher energies. This explanation even holds for the rest of the energy range. However, one can note the step in efficiency at about 10keV for the ER recoil and 15keV for the NR recoil. Let recall that the germanium crystal of RED80 was neutron-activated which results in a high rate of 10.37keV X-ray calibration events. These events are screening the events of energy lower than 10.37keV corresponding to 10.37keV for the ER recoils, and about 15keV (precision required here !!!) for the NR events. All-in-all, the asymptotic efficiency of the livetime cut is about 70% for the Background configuration, meaning that the detector is not available for proper data taking half the time! This is symptomatic from an above-ground experiment with minimal shielding which is subject to the natural radioactivity and cosmic rays inducing recoils triggering in the detector and screening other recoils. As for the Calibration configuration, this asymptotic efficiency is a lower 50% as the neutron source is facing the detector and adding to the total rate

of event in the detector.

Need to link this to the window length of 1s. Because a shorter window length would increase the livetime at the cost of the resolution i think.

The quality cut, defined in section 1.5 discards the events with a possibly problematic energy reconstruction. With this added cut, the efficiency drops to approximately 13% for the Background configuration and 3% for the Calibration configuration. We also note that the step assigned to the screening by the 10.37keV calibration events has vanished. This is explained by considering that all the events presenting a pile-up effect (usually with a 10.37keV X-ray recoil) were discarded, as mentioned in section 1.5. As the total event rate is higher for the Calibration configuration, the pile-up effect affects more events and thus the quality cut is pruning more than for the Background configuration.

The charge conservation cut effect seems marginal for the NR recoils and the lower-half of the energy range in the case of ER recoils. The slight suppression of the higher-half of the ER recoils spectra could be attributed to a more significant trapping of the electric charges in the crystal (see Chapter ??).

The fiducial cut then comes into play and have a significant effect on all the energy range for each combination. As defined in section 1.9, this cut selects the fiducial events happening in the bulk of the detector crystal. The efficiency is reduced by a factor 2/3 (precision necessary, associated plot is welcome), which could be attributed to fiducial volume of RED80 (link with chapter Electrodes ?).

Finally, the band cut, defined in section 1.10, seems to discard a negligible fraction of the events. This is to be associated with the figure 1.15 and figure 1.14: a majority of the events are allocated to either the ER or NR bands, with only a few events kept out.

With the obtainment of the efficiency as a function of the recoil energy for ER and NR recoils in the two configuration, Background and Calibration, it is now possible to correct the counts of the energy spectra. The histogram of the events passing all the cuts presented in figure 1.18, with a count m_i^A in the i -th bin for combination A is corrected into \mathcal{M}_i^A , the estimated number of recoils in the detector according to the following equation:

$$\mathcal{M}_i^A = \frac{m_i^A}{Eff_i^A} \quad (1.35)$$

is the a new energy spectrum necessary here ?

We could redraw energy spectra corresponding to this newly estimated number of recoils in the detector. However, the amount of events depends on the exposure of the detector as well as the presented data analysis. Normalization of the histogram is necessary to expressed the measurements independently from the experimental setup and the analysis.

1.15 Normalization of the energy spectra

From experimental data taken with the detector RED80 over a time span of several days, and with a proper processing and analysis of this data, we were able to estimate the number of electronic recoils and nuclear recoils that happened in the detector. The amount of recoil does depend on the nuclear and electronic background associated with the experimental setup which we want to measure. Yet, it is also proportional to the exposure of the detector as well as the bin width considered for the analysis. The bin width W_i was previously discussed in section 1.13 and is used now for this normalization.

The exposure corresponds to the mass of the germanium crystal: $m_{Ge} = 38g = 0.038kg$ multiplied by the running time of RED80. The latter was calculated in the table 1.2 with a period of $T^{Calibration} = 75.60\text{hours} = 3.150\text{days}$ for the Calibration configuration and $T^{Background} = 35.93\text{hours} = 1.497\text{days}$ for the Background configuration. These time length were obtained

by removing periods where the detector was not taking data, considering only the livetime as discuss in section 1.3.

The presentation of the measurement of the neutron and electronic background is done with the "event rate" quantity expressed in events/kg/keV/days. The event rate \mathcal{R}_i^A in the i -th bin for the combination A is expressed as:

$$\mathcal{R}_i^A = \frac{\mathcal{M}_i^A}{m_{Ge} \times T^A \times W_i} \quad (1.36)$$

with \mathcal{M}_i^A the estimated number of recoils (from equation 1.35).

The four event rates corresponding to each combination of recoil type and configuration are presented in figure 1.23. The event rates associated with the neutron background recoils are plotted in deep blue and light sky blue for the Calibration and the Background configuration respectively. We see that the event rate of the Calibration is two order of magnitude higher than for the Background configuration. The reference value is the event rate level at the lowest energies, which is about 10^5 Counts/keV/kg/days for the Calibration and 10^3 for the Background. This is expected (and reassuring) as the AmBe neutron source was only irradiating the detector during the Calibration configuration. Both event rates follows a "kinematic recoil distribution" (precision necessary here!!) as expected from thermalized neutron background (ref necessary).

The event rates corresponding to electronic recoil background is plotted is red and orange for the Calibration and Background configuration respectively. As expected, the ER background follow a mixture distribution whose components are the normal distribution of the 1.3keV and 10.37keV calibration lines of the germanium and the uniform distribution of the Compton background. We see that while the amplitude of the calibration peaks is approximately the same for both configurations, the flat Compton background is greater by a factor two for the Calibration compared to the Background. This can be explained by the higher neutron flux which produces gamma rays by interacting with the lead shielding of the cryostat.

Comparing the nuclear recoil background and the electronic recoil background, we see that the NR recoil is predominant over the Compton background from $\mathcal{O}(10\text{keV})$ in the Background configuration. This means that at higher energies, the main component of the energy spectrum is the Compton background, which is typically observe in the past Direct Dark Matter Searches. However, the neutron background is becoming the main component of the energy spectrum at lower energy. This means that by improving their energy resolution, the Direct Dark Matter experiments should now prepare for this new NR background and adapt their shielding.

1.16 Measurement of the ILL neutron background

The neutron background measurements at the IP2I cryostat with the RED80 38g germanium detector is used to extrapolate the neutron background that will affect the Cryocube array of germanium detector in the RICOCHET cryostat next to the nuclear reactor of the ILL. Indeed, the knowledge of this background is vital for RICOCHET as it is expected to constitute the main source of neutron recoil events that will screen the nuclear recoil coming from the CENNPs process.

While the neutron background was measured at the ILL with He3 detectors (with multiple nuclear reactor activities), this technology is only sensitive to energies higher than $\mathcal{O}(100)\text{keV}$. A way to link the neutron background at high energy with the neutron background at low energy is to measure the same neutron background with the two technologies of detectors. This reference neutron background measurement is the one at the IP2I cryostat facility. Measurement at low energy was presented in this section while measurement at high energies were taken with the He3 detector in place of the cryostat, with the same positions of the AmBe neutron source, leading to the two Calibration and Background configuration.

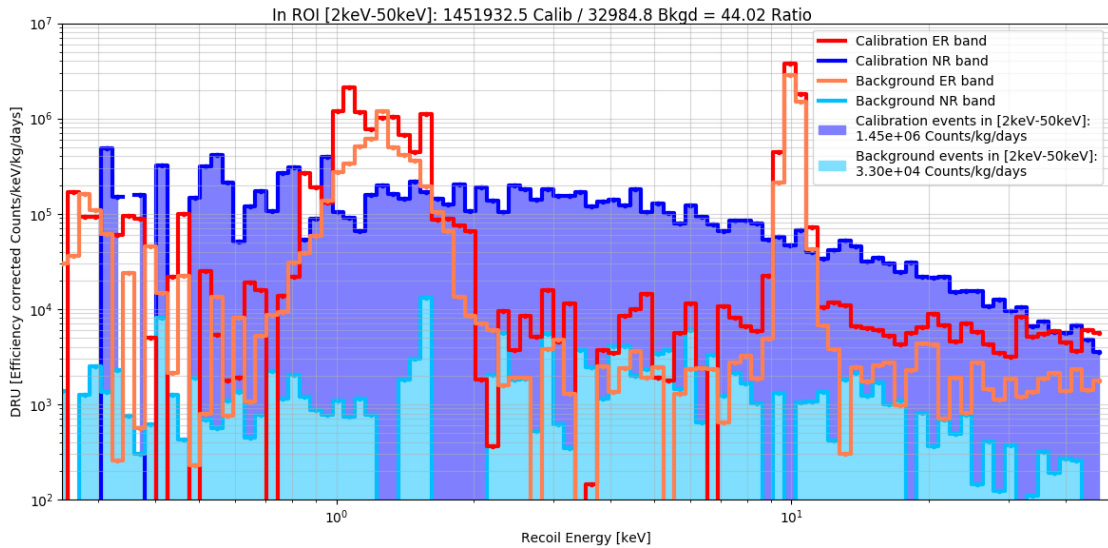


FIGURE 1.23: Normalized Recoil energy spectrum of the ER and NR band for the Calibration and the Background configurations.

The comparison of the high and low energy spectra should be relative (why?) between the Calibration and the Background configuration. For this, we use the nuclear recoil event rate of both configuration integrated of an energy span. The ratio of the integration in the interval [2 – 50]keV of the nuclear recoil energy spectra in Calibration and Background is:

$$\mathcal{R}_{[2-50]} = \frac{1.45 \times 10^6 \text{ Calibration events}}{3.30 \times 10^4 \text{ Background events}} = 44.02 \quad (1.37)$$

The ratio obtained by the He3 detectors were:

$$\begin{aligned} \mathcal{R}_{\text{Dubna3-He}} &= 26.5 \pm 4.8 \\ \mathcal{R}_{\text{Grenoble3-He}} &= 34.5 \pm 0.5 \end{aligned} \quad (1.38)$$

Interpretation, conclusion... Waiting for the final result for my analysis.

$$E_R = E_{\text{kin}}^N \frac{4m_N m_{Ge}}{(m_N + m_{Ge})^2} \cos^2(\theta) \approx E_{\text{kin}}^N \frac{4m_N}{m_{Ge}} \cos^2(\theta) \approx \frac{4}{73} E_{\text{kin}}^N \cos^2(\theta) \approx \frac{1}{20} E_{\text{kin}}^N \cos^2(\theta) \quad (1.39)$$

This equation means that a neutron with a kinematic energy of $E_{\text{kin}}^N = 200\text{keV}$ can produce at most a nuclear recoil of energy $E_R = 10\text{keV}$.

1.17 Study of the Heat-Only events

Work ongoing, Coming soon! free DLC The Heat-only events can be induced by several known process:

- recoil in the NTD passing the Quality cuts (usually at the lowest energy)
- event with a quenching factor $Q = 0$ induced by a surface electronic recoil (usually a electron from a β decay)

However, these processes alone can not explain the observations. Some ideas:

- crystal cracks

- release of energy stocked by inelastic nuclear recoil in the crystal lattice
- ???

1.18 Rejection and Leakage